Ore Geology Reviews 75 (2016) 327–344

Contents lists available at ScienceDirect

Ore Geology Reviews

journal homepage: www.elsevier.com/locate/oregeorev

The origin of the Dapingzhang volcanogenic Cu–Pb–Zn ore deposit, Yunnan province, SW China: Constraints from host rock geochemistry and ore Os–Pb–S–C–O–H isotopes

Wei-Guang Zhu [a], Hong Zhong [a,*], Yi-Jin Yang [a,b], Tao Ren [a,c]

[a] State Key Laboratory of Ore Deposit Geochemistry, Institute of Geochemistry, Chinese Academy of Sciences, 99 West Lincheng Road, Guiyang 550081, China
[b] University of Chinese Academy of Sciences, Beijing 100049, China
[c] Faculty of Land Resources Engineering, Kunming University of Science and Technology, Kunming, Yunnan 650093, China

ARTICLE INFO

Article history:
Received 10 August 2014
Received in revised form 9 December 2015
Accepted 13 December 2015
Available online 15 December 2015

Keywords:
Arc magmatism
S–Pb–C–H–O isotopes
Pyrite Re–Os isotope
VMS Dapingzhang Cu–Pb–Zn deposit
SW China

ABSTRACT

The Dapingzhang volcanogenic Cu–Pb–Zn sulfide deposit is located in the Lancangjiang tectonic zone within the Sanjiang region, Yunnan province of southwestern China. The deposit occurs within a felsic volcanic dome belonging to a mid-Silurian volcanic belt stretching for more than 100 km from Dapingzhang to Sandashan. The mineralized volcanic rocks are predominantly keratophyre and quartz keratophyre with subordinate spilite. The Dapingzhang deposit is characterized by well-developed vertical zonation with stockwork ores in the bottom, disseminated sulfide ores in the middle, and massive sulfide ores in the top, overlain by a thin layer of chemical sedimentary exhalative rocks (chert and barite). The Re–Os age of the pyrites from the deposit is 417 ± 23 Ma, indistinguishable from the age of the associated felsic volcanic rocks. The associated felsic volcanic rocks are characterized by negative Nb–Ta anomalies and positive $\varepsilon_{Nd}(t)$ values (+4.4–+6.5), similar to the coeval calc-alkaline volcanic rocks in the region. This observation supports the interpretation that the felsic volcanic rocks associated with the Dapingzhang deposit are the derivatives of arc basaltic magma by extensive fractional crystallization. The $\delta^{34}S$ values of the sulfides from the deposit vary from −1.24 to +4.32‰, indicating a predominantly magmatic source for the sulfur. The sulfides are also characterized by homogeneous and relatively low radiogenic Pb isotope compositions ($^{206}Pb/^{204}Pb$ = 18.310–18.656, $^{207}Pb/^{204}Pb$ = 15.489–15.643 and $^{208}Pb/^{204}Pb$ = 37.811–38.662), similar to the Pb isotopic compositions of the associated volcanic rocks. The Pb isotopic data indicate that mantle-derived Pb is more prevalent than crust-derived Pb in the deposit. The S–Pb isotopic data indicate that the important ore-forming materials were mainly derived from the associated volcanic rocks. The $\delta^{13}C_{PDB}$ and $\delta^{18}O_{SMOW}$ values of the associated hydrothermal calcite crystals vary from −2.3‰ to +0.27‰ and from +14.6 to +24.4‰, respectively. These values are between the mantle and marine carbonate values. The narrow range of the $\delta^{13}C_{PDB}$ values for the calcite indicates that carbon-bearing species in the hydrothermal fluids were primarily derived from marine carbonates. The $\delta^{18}O$ values for the hydrothermal fluids, calculated from the measured values for quartz, are between −2.1‰ and +3.5‰. The corresponding δD values for the fluids range from −59‰ to −84‰. The O–H isotopic data indicate mixing between magmatic fluids and seawater in the ore-forming hydrothermal system. Similar to a typical volcanogenic massive sulfide (VMS) deposit, the ore-forming fluids contained both magmatic fluids and heated seawater; the ore metals and regents were derived from the underlying magma as well as felsic country rocks.

1. Introduction

The Dapingzhang Cu–Pb–Zn ore deposit is mainly hosted in the felsic volcanic rocks of the Longdonghe Formation located in the Lancangjiang zone within the Sanjiang region, Yunnan province, southwest China. This province is a part of the Lanping–Simao Block at the southern margin of the Yangtze Block (Fig. 1). The volcanic host-rock sequence was previously assumed to have a Carboniferous age and was mapped as such in the regional geological maps of various scales (YBGMR, 1990, 2001). The studies on the Dapingzhang deposit are mostly available in Chinese only. However, the origin and evolution of hydrothermal fluids and the timing of mineralization have long been a matter of debate. This deposit was thought to be syngenetic with the hosting strata and to have formed as a typical volcanogenic massive sulfide (VMS)-type deposit (Li et al., 2000; Li and Zhuang, 2000, 2001; Zhong et al., 2000, 2001). Alternatively, the deposits were thought to have formed during an epigenetic hydrothermal event (ca. 118 Ma) (Dai et al., 2004). Recent zircon U–Pb dating data for the felsic volcanic rocks and Re–Os isotopic

* Corresponding author.
E-mail address: zhonghong@vip.gyig.ac.cn (H. Zhong).

http://dx.doi.org/10.1016/j.oregeorev.2015.12.011
0169-1368/

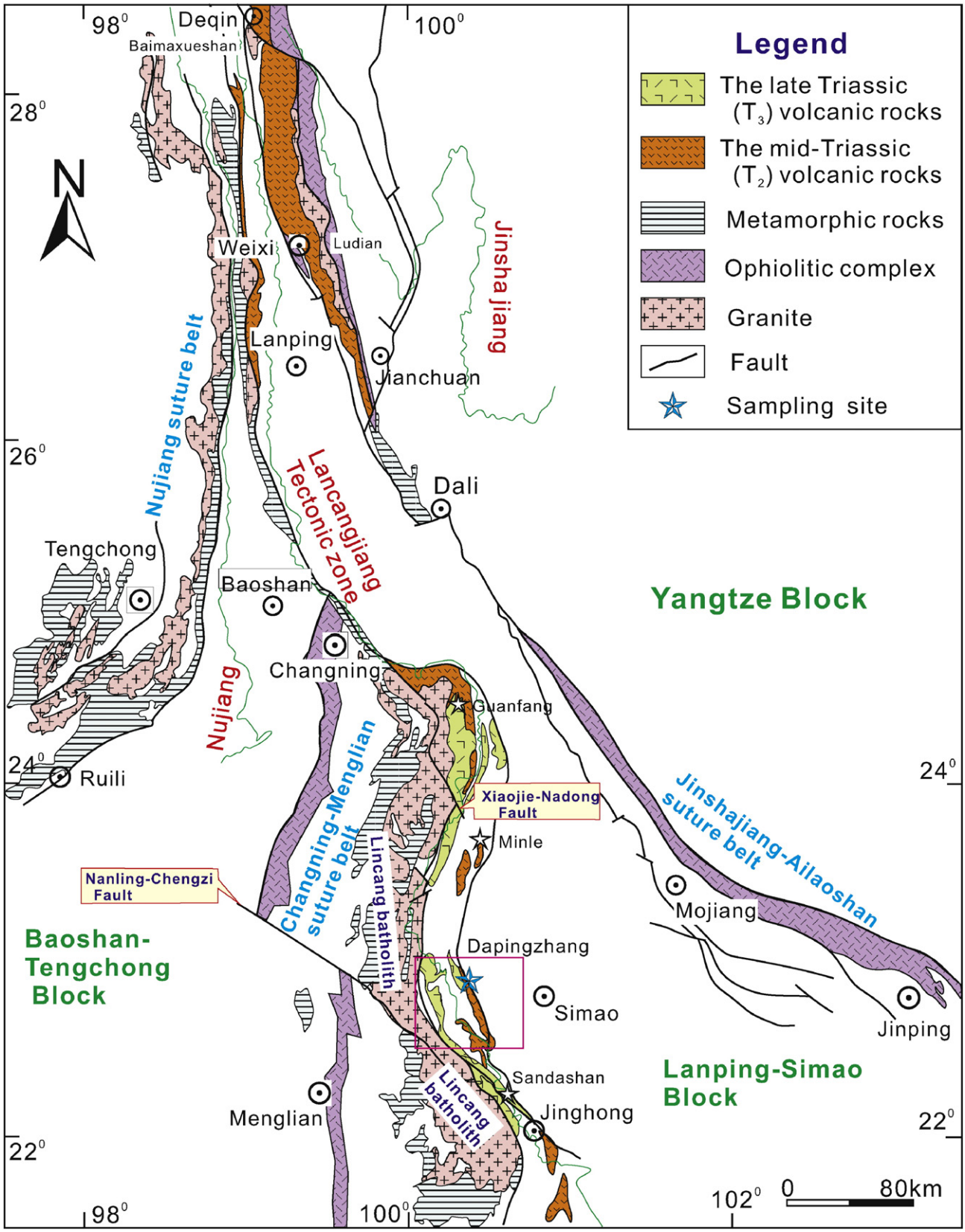

Fig. 1. Simplified geological map of the Sanjiang area in SW China.
Modified after YBGMR (1990), Peng et al. (2013) and Wang et al. (2014).

ages of bulk-rock ore samples indicate that they formed in the mid-Silurian (ca. 430 Ma) (Lehmann et al., 2013). Thus, the Dapingzhang volcanic sequence and associated Cu–Pb–Zn sulfide mineralization are different in time and geotectonic setting from other middle- to late-Triassic Cu polymetallic sulfide deposits in the west of the Lanping–Simao Block in western Yunnan, such as the Minle Cu deposit, the

Guanfang Cu–Pb deposit, and the Wenyu Cu deposit (Yang, 2003, 2004; Zhu et al., 2011; Chen et al., 2013).

The Triassic volcanoclastic rocks are widespread in the Lancangjiang zone (Peng et al., 2008, 2013; Wang et al., 2010). The early Paleozoic volcanic rocks in the Lancangjiang zone, west of the Changning–Menglian suture belt, have been gradually identified (Mao et al., 2012; Lehmann et al., 2013). In addition, recent zircon U–Pb data show that the cumulative gabbro and gabbro within the Nantinghe ophiolite in the northern part of the Changning–Menglian suture zone formed ca. 444–439 Ma (Wang et al., 2013), suggesting that the Paleo-Tethys oceanic basin was opened during the early Paleozoic. Understanding the formation of the early Paleozoic volcanic rocks in the Lancangjiang zone is thus crucial to illustrate the tectonic evolution of the main Paleo-Tethys Ocean.

In this study, we describe the geology of the Dapingzhang Cu–Pb–Zn ore deposit and report new S–Pb isotopes of sulfide minerals, C–O isotopes for hydrothermal calcite crystals, and H–O isotopes for hydrothermal quartz grains. New Re–Os isotopic dating of pyrite grains provides tight constraints on the timing of the main Cu–Pb–Zn mineralization. These new results are used to constrain the sources of the ore-forming fluids and metals and the age of the Cu–Pb–Zn mineralization. Furthermore, comprehensive analyses of elemental and Sr–Nd isotopic compositions have been conducted on the associated volcanic rocks hosting the Dapingzhang deposit. The aims are to constrain the origin of the volcanic rocks and elucidate the tectonomagmatic setting for the Dapingzhang deposit. Our results confirm that the Dapingzhang Cu–Pb–Zn ore deposit was formed in a typical volcanogenic hydrothermal fluid system.

2. Geologic background

The Sanjiang area (also referred to as the Three-River area because it includes the Jinsha, Lancang and Nu rivers) in western Yunnan province (Fig. 1) is an important region in the eastern Paleo-Tethys tectonic zone. Several Paleozoic sutures in the region provide a record of the history of the Paleo-Tethys Ocean, which consists of three paleo-oceanic basins known as the Jinshajiang, Lancangjiang, and Changning–Menglian Oceans from east to west (Mo et al., 1993; Pan et al., 2002, 2003; Mo and Pan, 2006; Jian et al., 2009a, 2009b). It includes high-pressure glaucophane schist, ophiolitic suites, mélange, and ocean island-, ocean ridge- and arc-related igneous rocks, and some back-arc rock associations (Zhang et al., 1985, 1988; YBGMR, 1990; Mo et al., 1998; Zhong, 1998; Jian et al., 2003, 2004, 2008, 2009a, 2009b; Fan et al., 2010; Wang et al., 2013, 2014). It is well documented that these remnants of the main Paleo-Tethys oceanic crust extend southward through Thailand to the Malay Peninsula and Sumatra.

The Lancangjiang (Lancang River) tectonic zone is located in the central part of the Sanjiang orogenic belt (YBGMR, 1990; Mo et al., 1998; Zhong, 1998). To its east lies the Lanping–Simao Block and further east is the Jinshajiang–Ailaoshan suture belt (Fig. 1). The Jinshajiang–

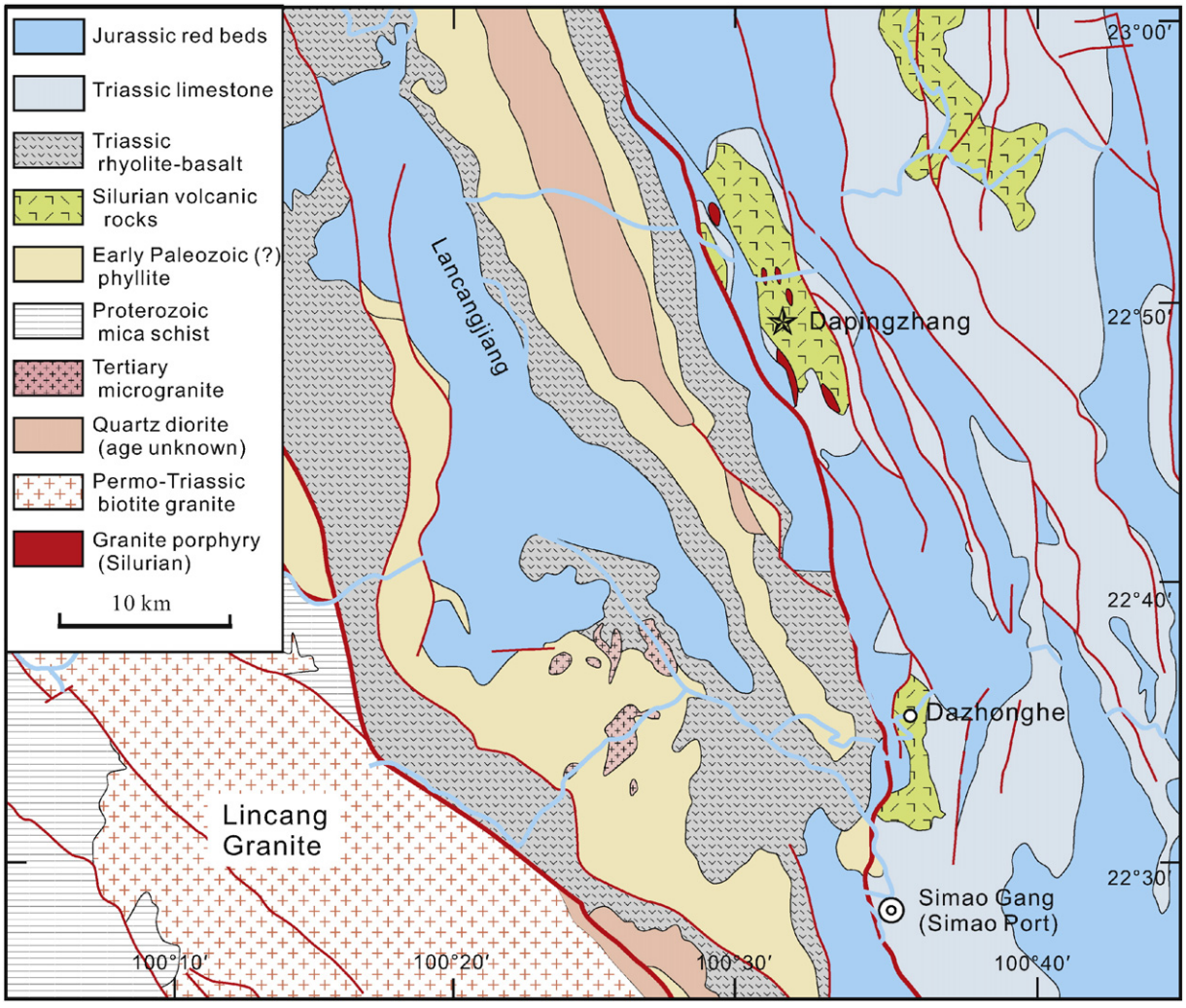

Fig. 2. Geological map of the Dapingzhang area based on YBGMR (2001). The Dapingzhang Cu–Pb–Zn ore deposit is hosted in a mid-Silurian volcanic sequence (ca. 429 Ma; Lehmann et al., 2013) and the Dazhonghe basaltic andesite to andesite (ca. 421–417 Ma; Mao et al., 2012) is exposed in the core of NW-trending anticlinal horst structures.

Ailaoshan suture belt is characterized by gabbro, anorthosite, and MORB dated at 387–374 Ma, which represents a back-arc ocean basin of the Paleo-Tethys (Jian et al., 2009a). To the west of the Lancangjiang tectonic zone is the Changning–Menglian suture zone and the Baoshan–Tengchong Block (Metcalfe, 2002) (Fig. 1). The basement rocks in the Lancangjiang area are the Proterozoic metasedimentary rocks of the Lancang, Chongshan, and Damenglong groups (Fig. 1). The Lancang Group lies to the west of the Lincang batholith and consists of sandstones, mudstones, slates, phyllites, and minor chlorite schists and blueschists. The Chongshan and Damenglong groups are to the east of the Lincang batholith, comprising banded gneiss, quartzo-feldspathic mica schist, amphibolite, migmatite, and marble (Zhao, 1990; Zhong, 1998; Heppe, 2004). All three groups have undergone several stages of metamorphism and deformation (Zhong, 1998; Heppe, 2004). The Lancangjiang tectonic zone includes the early Permian Banpo mafic–ultramafic complex dated at 288–284 Ma (Jian et al., 2009a) or 295 Ma (Li et al., 2012) and the Nanlianshan mafic–ultramafic volcanoplutonic complex dated at 298–292 Ma (Hennig et al., 2009; Li et al., 2012). The southern Lancangjiang zone in SW China consists of the Lincang batholith and the Triassic volcanic belt (Fig. 1; Peng et al., 2006, 2008, 2013; Wang et al., 2010). Detailed information on the regional geology and precise dating of magmatic events in the area has been summarized in Jian et al. (2009a, 2009b).

The Changning–Menglian suture zone represents the remnant of the main Paleo-Tethys oceanic crust in SW China and extends southward into Southeast Asia, including the Inthanon and Bentong–Raub suture belts (Metcalfe, 2002, 2011; Zhong, 1998). The timing of the formation of the Changning–Menglian suture zone has great significance in the evolution and paleogeographic reconstruction of the Paleo-Tethys Ocean. However, the opening time of the Paleo-Tethys Ocean basin, represented by the Changning–Menglian suture zone, is still debated. Some researchers have suggested that the Changning–Menglian Ocean basin formed during the early Carboniferous, based on the oceanic island-type and MORB-type basalts from the Pingzhang Formation of the

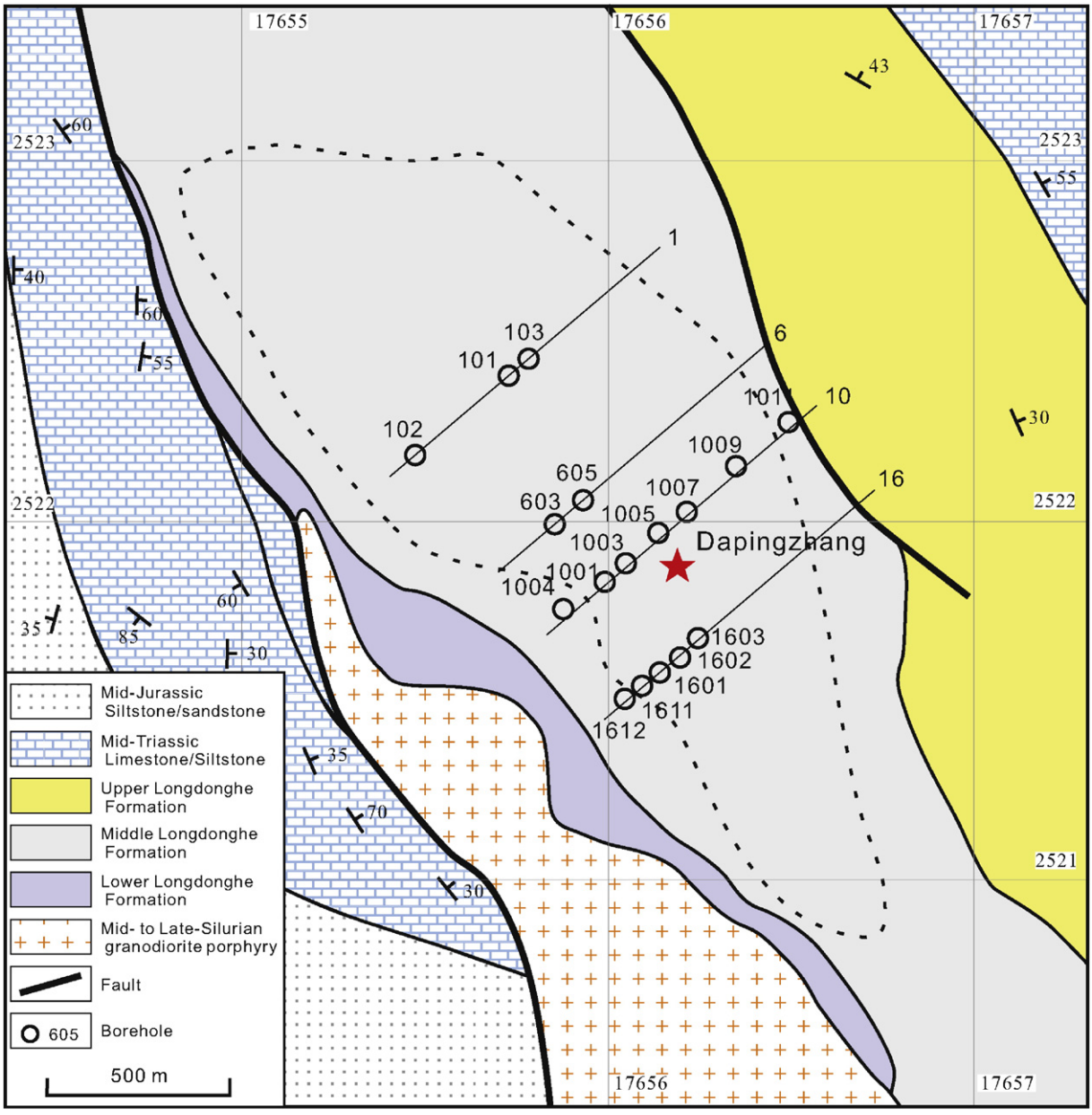

Fig. 3. Local geology of the Dapingzhang volcanic-hosted Cu–Pb–Zn ore deposit.
Modified after Li et al. (2000).

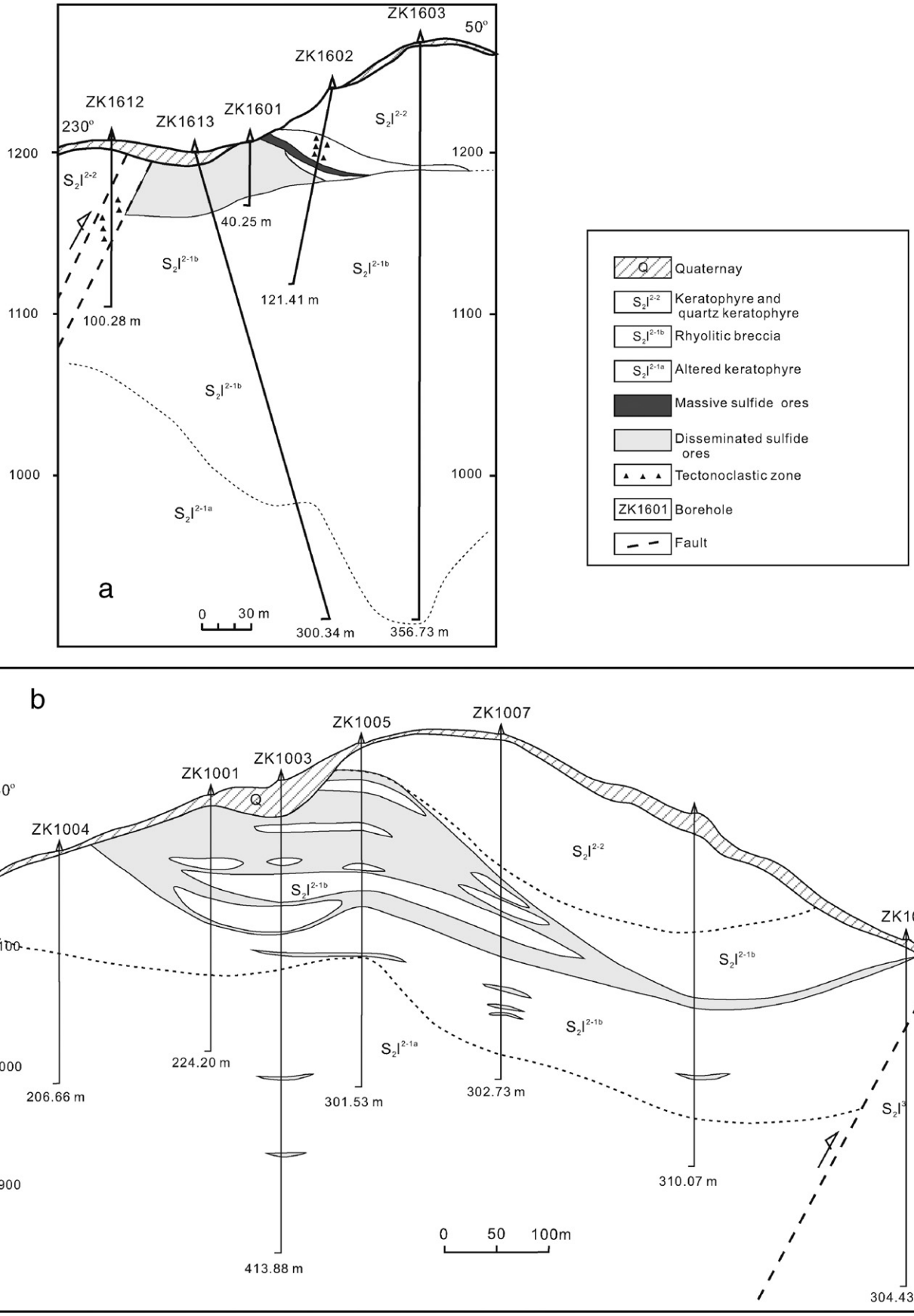

Fig. 4. The cross-sections of exploration line 16 (a) and line 10 (b) of the Dapingzhang Cu–Pb–Zn ore deposit (after Li et al., 2000; Yang and Hu, 2001), which includes both massive sulfide ores and dominant disseminated ores.

Lower Carboniferous (Shen et al., 2002). On the other hand, according to the isotopes of volcanic rocks from the Tongchangjie, some proposed that it formed during the Devonian (Zhong et al., 1998). Yang et al. (2007) also thought that it formed during the Devonian, based on the associated late Devonian radiolarians and conodonts in the siliceous and siliceous mudstone occurring with the pillow basalts in the Changning–Menglian suture zone from the Gengma area in western Yunnan. However, recent LA-ICP-MS zircon U–Pb dating indicates that the cumulative gabbro and the Nantinghe ophiolite gabbro formed 444–439 Ma, implying that the early Paleozoic ophiolites occurred in the Changning–Menglian zone (Wang et al., 2013). The Nantinghe ophiolite can integrate with the Guoganjianianshan and Taoxinghu ophiolites in the Qiangtang region (Li et al., 2008; Wang et al., 2008; Zhai et al., 2010). This finding suggests that they represent the early Paleozoic fragments of oceanic crust of the uniform Paleo-Tethys.

3. Local and deposit geology

The Dapingzhang deposit is located along the margin of the Mesozoic–Cenozoic Simao basin (Fig. 1). The basement of this basin is only exposed near its margins and in a few fault-bounded anticlines or horst structures. The deposit is in the core of such an anticline/horst (Fig. 2). The tectonic windows represented by the Dapingzhang anticline, the Yunxian anticline 15 km to the east, and the Yinzishan anticline 25 km to the south, expose a volcaniclastic sequence possibly >2000 m in thickness (Yang et al., 2000). The basement rocks in the Dapingzhang area are the Proterozoic meta-sedimentary rocks of the Chongshan Group, consisting of metamorphosed quartz-feldspathic mica schist, banded gneiss, and amphibolite. The early Paleozoic strata are predominantly comprised of phyllite and the ca. 430–420 Ma volcanic rocks consisting of basaltic, andesitic, dacitic, and rhyolitic rocks (Mao et al., 2012; Lehmann et al., 2013). The middle to late Triassic

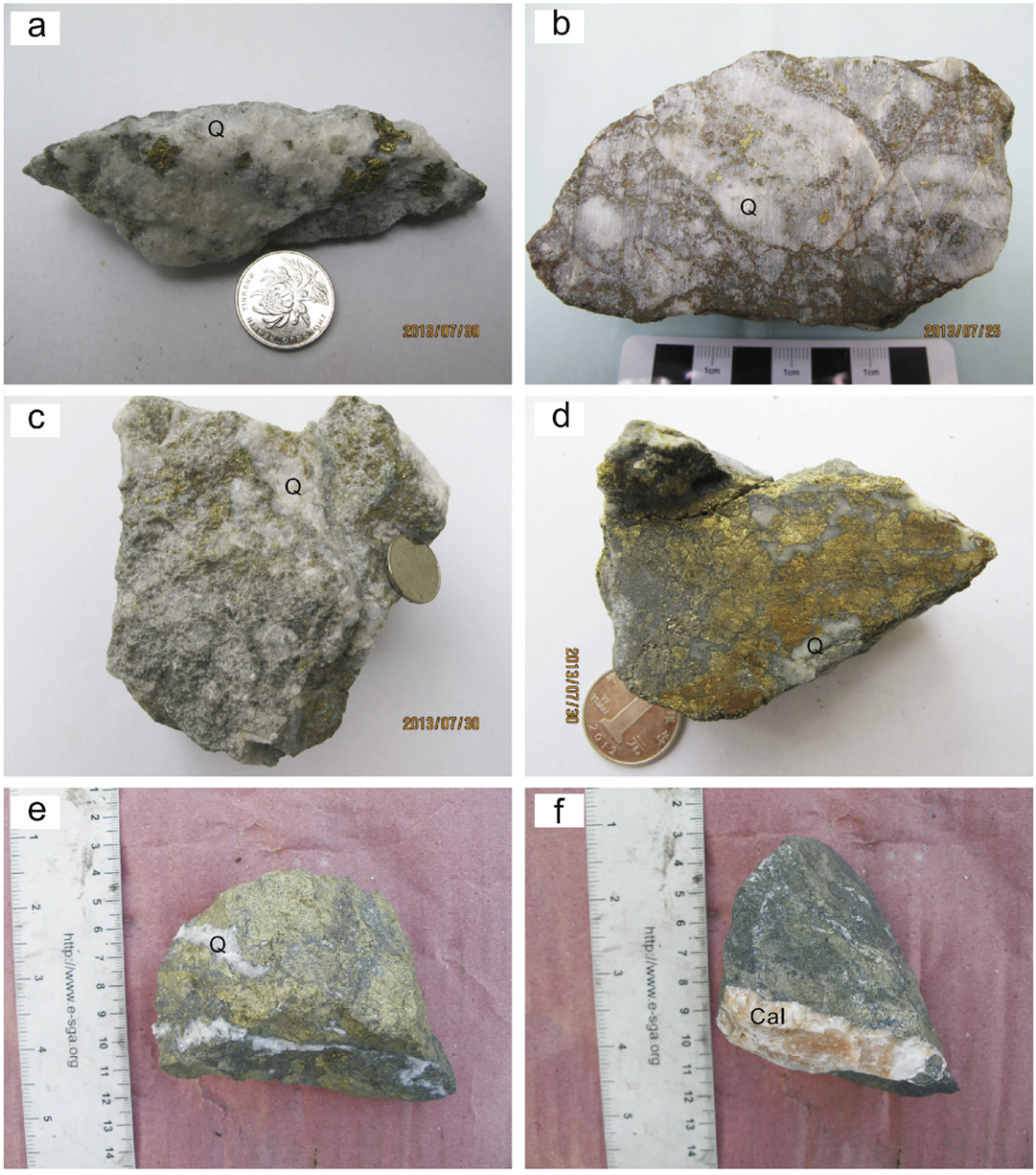

Fig. 5. Photographs of the typical sulfide ore textures from the Dapingzhang Cu–Pb–Zn ore deposit. (a) Disseminated sulfide ores: euhedral or subhedral sulfide (pyrite, chalcopyrite) grains within the massive quartz vein. (b) Disseminated sulfide ores: disseminated sulfides (pyrite, chalcopyrite) within the brecciated quartz grains. (c) Disseminated sulfide ores: disseminated sulfides (pyrite, chalcopyrite) within the altered rhyolitic rocks and quartz veins. (d) Massive sulfide ores and irregular quartz veins. (e) Massive sulfide ores and quartz veins. (f) Massive sulfide ores and calcite vein. Q–quartz, and Cal–calcite.

Table 1
Major element (in wt.%) and trace element (in ppm) compositions of volcanic rocks associated with the Dapingzhang Cu–Pb–Zn ore deposit.

Sample no.	DPZ0904	DPZ0905	DPZ0907	DPZ0908	DPZ0909	DPZ0910	DPZ0911	DPZ0912	DPZ0913	DPZ0914	DPZ0915	DPZ0916	DPZ0917	DPZ0918	DPZ0919	DPZ0920	DPZ0921
SiO_2	70.62	71.78	73.08	74.56	71.61	73.33	72.81	72.85	72.58	72.93	72.06	71.05	71.65	71.79	72.19	73.09	74.49
TiO_2	0.34	0.32	0.33	0.32	0.32	0.32	0.32	0.34	0.34	0.32	0.34	0.33	0.33	0.36	0.32	0.32	0.35
Al_2O_3	13.50	13.10	13.34	12.53	13.06	13.15	13.15	12.99	13.69	13.29	13.50	13.32	13.66	12.99	13.34	13.01	12.73
Fe_2O_3	4.62	4.16	3.38	3.21	3.51	3.42	3.20	3.79	3.40	3.20	3.45	3.53	3.80	3.55	3.53	3.64	3.28
MnO	0.11	0.10	0.09	0.10	0.12	0.12	0.11	0.09	0.07	0.08	0.10	0.10	0.10	0.11	0.11	0.12	0.08
MgO	1.90	2.70	2.37	2.21	2.34	2.15	2.53	2.09	1.80	1.83	2.43	2.73	2.32	2.27	2.54	2.20	1.85
CaO	0.87	0.40	0.16	0.18	1.03	0.21	0.19	0.52	0.40	0.71	0.40	1.03	0.41	0.77	0.35	0.27	0.19
Na_2O	4.47	4.04	3.05	3.53	3.50	3.21	3.83	3.37	3.93	4.24	3.93	2.98	3.45	3.51	3.93	4.38	3.48
K_2O	0.73	0.73	1.58	1.03	1.26	1.42	1.00	1.30	1.30	0.99	1.15	1.54	1.48	1.22	1.12	0.66	1.29
P_2O_5	0.07	0.07	0.07	0.07	0.07	0.07	0.07	0.07	0.07	0.07	0.07	0.07	0.07	0.07	0.07	0.07	0.06
LOI	2.49	2.43	2.39	2.17	3.04	2.30	2.24	2.41	2.11	2.21	2.37	3.15	2.49	2.67	2.29	1.94	1.89
Total	99.72	99.83	99.84	99.91	99.86	99.70	99.45	99.82	99.69	99.87	99.80	99.83	99.76	99.31	99.79	99.70	99.69
$Mg^{\#}$	44.9	56.2	58.1	57.7	56.9	55.5	61.0	52.2	51.2	53.1	58.2	60.5	54.7	55.9	58.8	54.5	52.8
Sc	18.8	17.8	16.4	15.5	17.4	16.2	16.6	16.5	17.9	17.5	18.4	17.5	17.3	17.0	17.6	16.2	16.0
V	46.7	44.7	44.5	42.5	44.8	46.1	44.6	44.9	44.3	47.4	46.8	47.2	45.8	45.6	49.6	43.6	46.7
Cr	2.30	3.66	4.15	2.45	7.62	3.44	4.20	3.15	6.05	4.41	4.32	9.22	2.60	8.70	5.71	4.77	2.82
Co	10.8	4.10	3.50	2.17	3.56	5.86	3.80	4.79	4.60	3.69	3.70	4.34	4.44	3.67	4.15	3.64	4.60
Ni	1.51	2.40	1.69	1.22	4.41	2.04	2.35	1.16	1.89	2.40	2.13	4.12	1.77	4.75	3.22	1.92	1.90
Cu	7.46	8.50	43.4	5.81	165	5.77	5.34	2.66	4.45	2.48	3.88	5.03	230	5.90	5.26	17.6	5.20
Zn	41.7	68.3	61.8	52.5	54.6	162.8	91.2	67.5	51.2	50.0	61.7	63.0	65.5	60.2	65.1	123	69.2
Ga	12.4	12.4	12.6	11.4	12.2	12.2	11.9	12.4	12.5	12.7	12.1	12.6	12.5	12.0	12.7	11.5	12.4
Rb	11.7	11.7	24.4	15.4	21.1	21.5	15.8	20.9	21.9	14.7	20.6	24.7	23.8	19.0	18.2	10.3	19.0
Sr	96.4	77.3	78.1	80.4	115	94.5	72.4	93.1	103	110	96.1	100	111	98.9	110	102	42.6
Y	26.8	22.5	16.6	20.0	25.5	23.9	22.1	24.9	24.3	33.4	20.9	27.7	15.6	22.1	26.1	25.6	18.1
Zr	82.8	84.1	82.0	78.9	81.8	83.3	82.5	83.9	83.5	83.1	85.1	81.4	84.3	79.7	82.6	79.9	90.3
Nb	2.18	2.33	2.16	2.19	2.15	2.14	2.27	2.19	2.19	2.24	2.22	2.15	2.22	2.19	2.15	2.23	2.23
Cs	1.30	0.695	3.00	1.43	2.37	2.81	1.42	2.69	2.91	1.69	3.25	1.59	1.90	1.23	1.49	0.44	1.16
Ba	177	189	363	347	317	343	259	340	246	242	303	377	393	373	310	289	368
La	13.3	9.12	8.05	6.03	10.4	7.25	7.55	13.0	12.5	6.69	6.99	12.3	4.37	7.60	9.92	15.3	3.32
Ce	27.5	19.5	17.7	15.8	23.3	17.4	18.8	27.7	25.6	15.0	15.4	25.6	10.0	17.0	20.4	31.8	8.17
Pr	3.21	2.27	2.11	1.89	2.80	2.04	2.26	3.33	3.03	1.85	1.82	3.19	1.18	2.15	2.36	3.70	1.01
Nd	13.9	10.1	8.92	7.65	11.4	8.81	9.05	13.7	12.8	7.36	7.63	12.3	5.34	9.00	10.9	16.1	4.87
Sm	3.35	2.70	2.41	2.11	3.10	2.39	2.34	3.36	3.25	2.10	1.76	3.13	1.42	2.48	2.77	4.00	1.23
Eu	0.966	0.704	0.432	0.343	0.677	0.500	0.512	0.768	0.781	0.507	0.483	0.745	0.248	0.439	0.752	1.00	0.219
Gd	3.29	2.79	2.01	1.78	2.80	2.10	2.30	3.18	2.76	2.62	1.94	3.00	1.58	2.23	2.75	3.69	1.61
Tb	0.660	0.511	0.410	0.419	0.597	0.522	0.486	0.621	0.586	0.627	0.433	0.601	0.289	0.487	0.546	0.663	0.345
Dy	4.11	3.38	2.42	2.91	3.74	3.53	3.02	3.74	3.71	4.72	2.96	4.04	2.17	3.11	3.54	4.01	2.54
Ho	0.957	0.794	0.579	0.718	0.881	0.87	0.733	0.867	0.826	1.09	0.727	0.942	0.568	0.766	0.884	0.884	0.620
Er	3.03	2.62	1.94	2.18	2.70	2.64	2.46	2.56	2.74	3.43	2.32	3.09	1.85	2.50	2.75	2.65	2.01
Tm	0.472	0.408	0.324	0.349	0.445	0.409	0.401	0.381	0.424	0.536	0.383	0.439	0.298	0.390	0.421	0.371	0.318
Yb	3.17	2.66	2.28	2.34	2.88	2.79	2.64	2.63	2.80	3.32	2.54	3.05	2.35	2.68	2.75	2.71	2.15
Lu	0.497	0.417	0.371	0.372	0.462	0.46	0.395	0.424	0.452	0.517	0.457	0.496	0.392	0.410	0.463	0.408	0.394
Hf	2.25	2.41	2.47	2.17	2.16	2.39	2.51	2.42	2.30	2.31	2.48	2.57	2.44	2.18	2.35	2.33	2.62
Ta	0.133	0.129	0.114	0.113	0.103	0.12	0.123	0.104	0.117	0.102	0.109	0.124	0.133	0.118	0.122	0.102	0.106
Pb	3.75	1.55	1.48	3.73	1.57	6.69	3.47	2.72	1.55	1.20	1.75	1.89	1.74	1.53	1.54	1.75	1.58
Th	2.72	2.70	2.70	2.49	2.72	2.73	2.63	2.76	2.78	2.75	2.65	2.73	2.77	2.60	2.57	2.57	2.57
U	1.38	1.02	1.08	1.20	1.08	1.00	0.98	1.06	0.934	1.18	1.06	1.07	1.07	1.08	1.14	1.06	1.15

$Mg^{\#} = 100 * (MgO / (Mg + FeO))$, molar; total iron reported as Fe_2O_3; and LOI = loss on ignition.

stratum is mainly composed of volcanic rocks (basaltic and rhyolitic rocks), limestone, siltstone, and sandstone. The middle Jurassic stratum is composed of red-bed sediments (Figs. 2 and 3).

There are two major igneous rock units within the Dapingzhang ore district (Fig. 3): (1) the mid-Silurian volcanic rocks (spilite, keratophyre, and quartz keratophyre) of the Longdonghe Formation (Lehmann et al., 2013) and (2) the mid- to late-Silurian (ca. 401 Ma) granodiorite porphyry that intruded into the lower Longdonghe Formation (Ru et al., 2012). The north-west trending Longdonghe Formation is divided into three parts. The lower part mainly contains spilite, keratophyre, quartz keratophyre overlain by chert and tuff layers. The middle part consists of quartz- and feldspar-phyric keratophyre, dacitic to rhyolitic breccias, and volcaniclastic rocks interbedded with several spilite layers. The upper part is composed of keratophyre and quartz keratophyre interbedded with chert and siltstone layers. The volcanic rocks at Dapingzhang are discordantly overlain by middle Triassic clastic rocks and massive limestones, which are in turn unconformably overlain by Jurassic continental siltstone/sandstone (Li et al., 2000; Fig. 3).

The Dapingzhang deposit is located in the volcanic dome of the core of anticlines and is hosted by the middle part of the Longdonghe Formation (Fig. 3). The deposit contains approximately 43 Mt of ore at 1.20 wt.% Cu and 5 Mt of ore at 10.2 wt.% Pb + Zn with minor amounts of Au and Ag (Wang, 2004). In accordance with mineral association and ore structure, sulfide ores in the Dapingzhang deposit can be divided into three types: stockwork ores, disseminated sulfide ores, and stratiform massive sulfide ores. From the base to the top, the deposit displays a typical VMS vertical zonation of the chalcopyrite–pyrite stockwork ores, disseminated sulfide ores, stratiform massive sulfide ores, and a thin layer of chemical sedimentary exhalative rocks (chert and barite) in the hanging wall (Fig. 4; Li et al., 2000; Yang and Hu, 2001).

The disseminated sulfide ores are controlled by volcanic breccia pipes beneath several stratiform massive sulfide lenses. Generally, the approximately 200–700 m long and 50–540 m wide orebodies follow the general structure of the host rocks (NW), dipping to the northeast with an angle of ~6°–27°. The disseminated mineralizations are associated with the dacitic to rhyolitic breccias surrounded by several hundred-meter-wide altered rhyolitic rocks that are associated with the alteration of quartz, feldspar, calcite, and sericite and are overlain by relatively unaltered quartz- and feldspar–phyric keratophyre and quartz keratophyre (hanging wall). The footwall contact of the disseminated orebodies and the dacitic to rhyolitic breccias are gradational. Furthermore, there are a few steeply dipping Cu-rich stockwork orebodies beneath the disseminated sulfide ores. However, the contact between the disseminated orebodies and the hanging-wall rocks is sharply defined (Fig. 4; Li et al., 2000; Yang and Hu, 2001). The

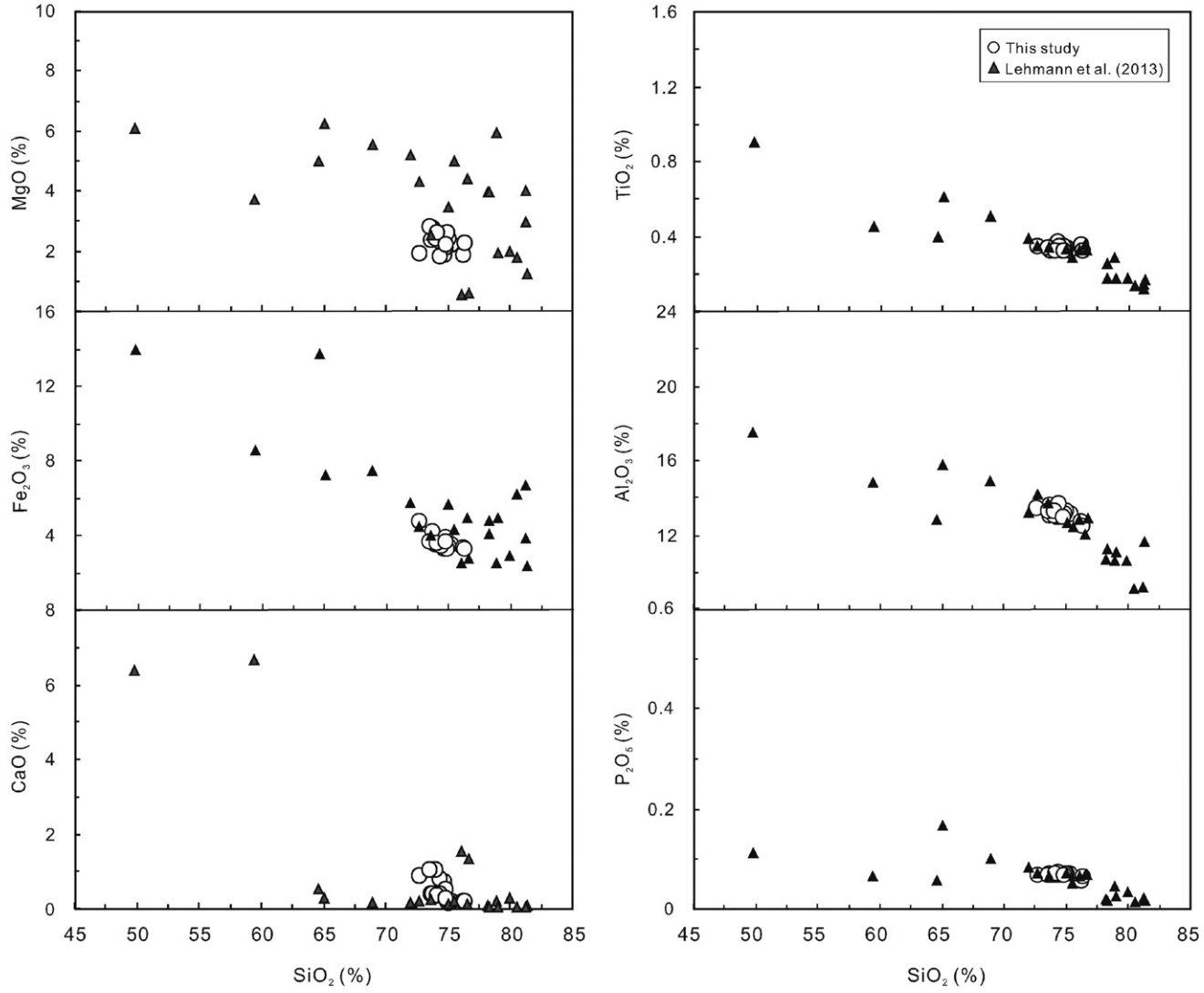

Fig. 6. Selected variation diagrams of major oxide (MgO, TiO_2, Fe_2O_3, Al_2O_3, CaO, and P_2O_5) contents and silica for the associated volcanic rocks from the Dapingzhang Cu–Pb–Zn ore deposit.

disseminated sulfide ores are dominated by ore minerals and >65% nonsulfide gangue. The principal ore minerals include dominant pyrite, chalcopyrite, minor sphalerite, and galena. The gangue minerals are mainly quartz, feldspar, sericite, and subordinate chlorite (Fig. 5a–c).

The stratiform massive sulfide ores are located within tectonoclastic zones that are related to the faults and overlie the disseminated ores in the pipe-like volcanic breccias. They trend north-west, with lengths generally ranging from 100 to 450 m and widths ranging from 80–260 m, dipping to the northeast with an angle of ~10°–27°. The lower contact between the massive ores and the disseminated ores is gradational, whereas the upper contact of orebodies against tectonoclastic rocks is sharp (Fig. 4a; Li et al., 2000; Yang and Hu,

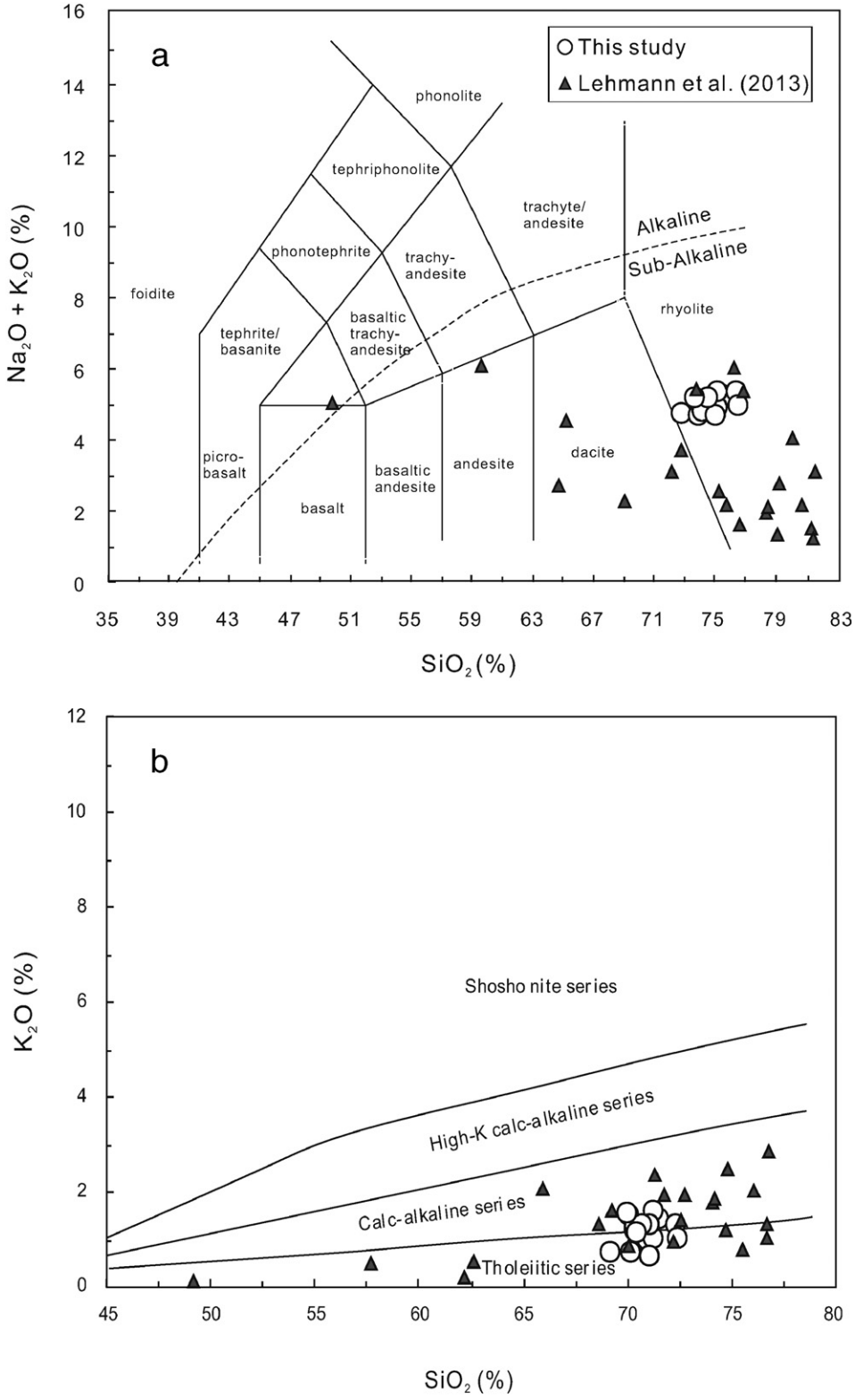

Fig. 7. (a) ($Na_2O + K_2O$) vs. SiO_2 classification diagram (Irvine and Baragar, 1971; Le Bas and Streckeisen, 1991) and (b) K_2O vs. SiO_2 diagram from Rickwood (1989) for the Dapingzhang volcanic rocks.

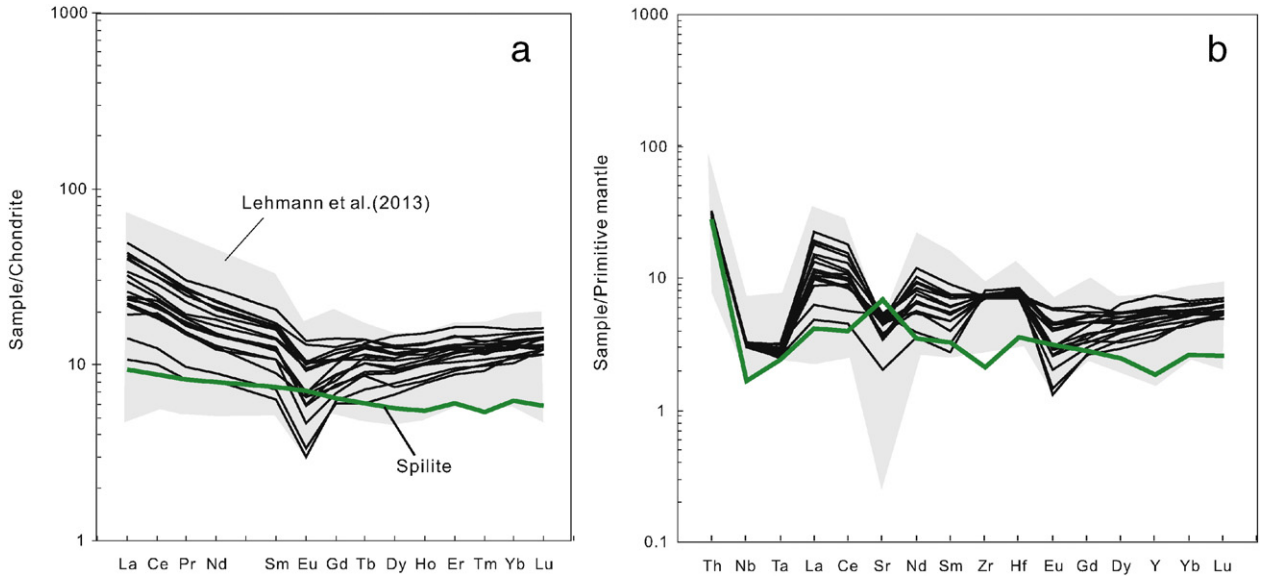

Fig. 8. (a) Chondrite-normalized REE diagram and (b) primitive mantle-normalized incompatible trace element multi-element plot for the volcanic rocks from the Dapingzhang Cu–Pb–Zn ore deposit. Chondrite-normalizing values are from Boynton (1984). Primitive mantle-normalizing values are from Sun and McDonough (1989).

2001). The massive sulfide lenses mainly consist of chalcopyrite, pyrite, sphalerite, and galena with <20% nonsulfide gangue. The gangue minerals mainly consist of quartz, calcite, chert, and barite (Fig. 5d–f).

4. Samples and analytical methods

4.1. Sample collection and preparation

Samples were collected from different ore types and positions in an open pit in the Dapingzhang deposit. To reduce possible alteration effects, the volcanic rock samples were mainly collected from the relatively unaltered quartz- and feldspar–phyric keratophyre and quartz keratophyre. Pure chalcopyrite, pyrite, sphalerite, quartz, and calcite minerals from the disseminated and massive sulfide ores were crushed to 40–80 meshes and were handpicked under a binocular microscope. The purity of a single mineral separate was greater than 99%. Pyrite, chalcopyrite, sphalerite, and galena minerals were analyzed for S–Pb isotopic compositions, quartz grains for H–O isotopic compositions, and calcite crystals for C–O isotope compositions.

4.2. Elemental and Sr–Nd isotopic analyses of the volcanic rocks

The major element compositions of the volcanic rocks were determined using an X-ray fluorescence spectrometer (XRF) at the ALS Mineral Laboratory, Guangzhou. The analytical precisions were better than 5%. Trace elements in whole rocks were analyzed using a Perkin-Elmer Sciex ELAN DRC-e ICP-MS at the State Key Laboratory of Ore Deposit Geochemistry (SKLOG), Institute of Geochemistry, Chinese Academy of Sciences (IGCAS), Guiyang. The powdered samples (50 mg) were dissolved in $HF + HNO_3$ mixtures in high-pressure Teflon bombs at ~190 °C for 48 h (Qi et al., 2000). Rh was used as an internal standard to monitor signal drift during measurement. The international standards GBPG-1 and OU-6 and the Chinese National standards GSR-1 and GSR-3 were used for analytical quality control. The analytical precisions were generally better than 10% for trace elements.

In the Sr–Nd isotopic analyses, the volcanic rocks were spiked and dissolved in Teflon bombs using an acidic mixture of HF, HNO_3, and $HClO_4$. Then, they were separated using conventional cation-exchange techniques. The isotopic measurements were performed on an MC-ICP-MS at the Key Laboratory of Orogenic Belts and Crustal Evolution, School of Earth and Space Sciences, Peking University. The mass fractionation corrections for the Sr and Nd isotopic ratios were based on values of $^{86}Sr/^{88}Sr = 0.1194$ and $^{146}Nd/^{144}Nd = 0.7219$, respectively. The determined $^{86}Sr/^{88}Sr$ ratio of the NBS987 Sr standard was 0.710250 ± 7 (2σ), and the $^{143}Nd/^{144}Nd$ ratios of the JNDI-1 Nd standard solution and the USGS standard rock BCR-2 were 0.512119 ± 14 (2σ) and 0.512629 ± 16 (2σ), respectively.

4.3. Re–Os dating of pyrites

Re–Os isotopic analyses of pyrite grains were performed at the SKLODG. Pyrite separates of 1 to 3 g were accurately weighed depending on the pre-analyzed Re contents of the samples and were digested in 120-ml Carius tubes using aqua regia with known amounts of rhenium and osmium spikes at 200 °C for approximately 10 h. Os was separated from the matrix by distillation, whereas Re was separated from the remaining solutions using an anion exchange resin. Re and Os isotope compositions were measured on an ELAN DRC-e ICP-MS with

Table 2
Sr and Nd isotopes of volcanic rocks associated with the Dapingzhang Cu–Pb–Zn ore deposit.

Sample No.	Rb (ppm)	Sr (ppm)	$^{87}Sr/^{86}Sr$ (2σ)	$(^{87}Sr/^{86}Sr)_i$	Sm (ppm)	Nd (ppm)	$^{143}Nd/^{144}Nd$ (2σ)	$(^{143}Nd/^{144}Nd)_i$	$\varepsilon_{Nd}(t)$
DPZ0904	10.8	85.6	0.709804 (19)	0.707636	3.32	12.9	0.512785 (12)	0.512348	5.13
DPZ0905	10.1	62.7	0.708955 (15)	0.706186	2.34	9.42	0.512774 (17)	0.512352	5.20
DPZ0908	14.7	69.1	0.709463 (17)	0.705807	1.67	6.84	0.512818 (19)	0.512403	6.20
DPZ0912	17.8	71.9	0.709254 (19)	0.704999	2.35	10.6	0.512745 (17)	0.512369	5.53
DPZ0913	19.0	85.8	0.709516 (17)	0.705711	2.84	11.6	0.512729 (19)	0.512313	4.45
DPZ0918	18.2	90.1	0.709637 (18)	0.706165	2.06	8.67	0.512718 (16)	0.512314	4.47
DPZ0919	17.0	92.5	0.708917 (16)	0.705759	1.88	7.55	0.512841 (17)	0.512418	6.50

Chondrite uniform reservoir (CHUR) values ($^{87}Rb/^{86}Sr = 0.0847$, $^{87}Sr/^{86}Sr = 0.7045$; $^{147}Sm/^{144}Nd = 0.1967$, $^{143}Nd/^{144}Nd = 0.512638$) are used for the calculation. $\lambda_{Rb} = 1.42 \times 10^{-11}$ year^{-1} (Steiger and Jäger, 1977); and $\lambda_{Sm} = 6.54 \times 10^{-12}$ year^{-1} (Lugmair and Harti, 1978). The $(^{87}Sr/^{86}Sr)_i$, $(^{143}Nd/^{144}Nd)_i$, and ε_{Nd} (t) were calculated using an age of 429 Ma.

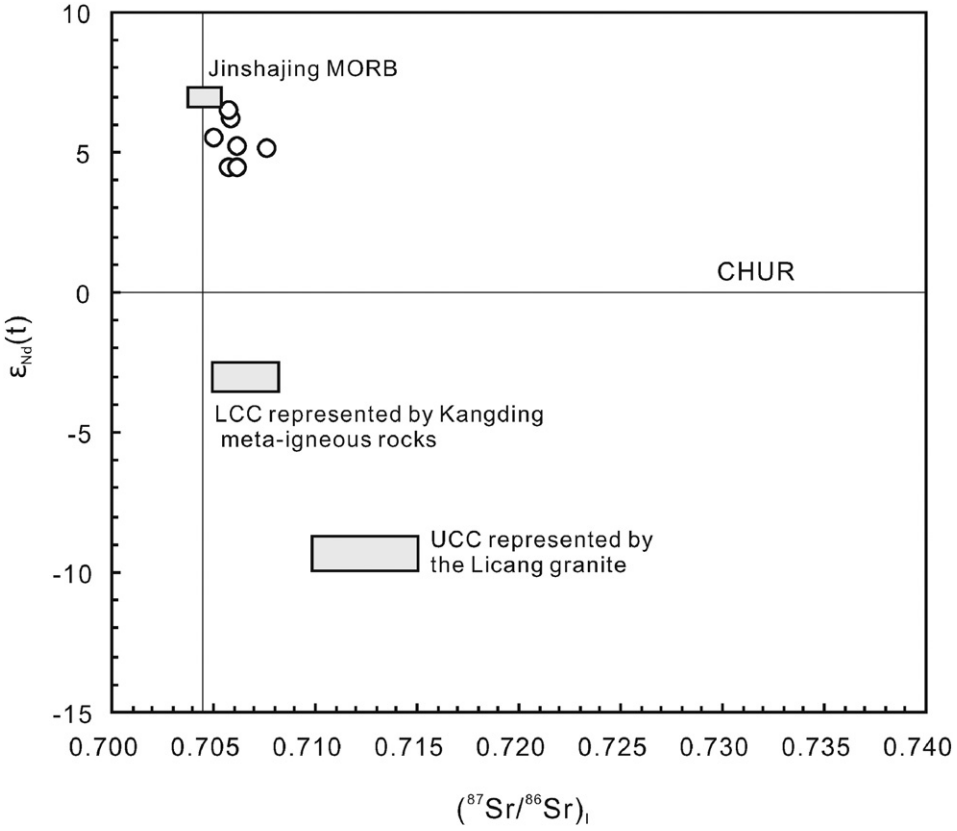

Fig. 9. $\varepsilon_{Nd}(t)$ vs. $(^{87}Sr/^{86}Sr)_i$ diagram of the volcanic rocks from the Dapingzhang Cu–Pb–Zn ore deposit. All of the initial isotopic ratios were corrected to 429 Ma. The Jinshajiang MORB from Xu and Castillo (2004), Kangding complex from Chen et al. (2001), Sr isotopic data of the Lincang granites from Liu and Zhu (1989), and Nd isotopic data of the Lincang granites from Lehmann et al. (2013).

total blanks of 6.4 pg Re and 2.0 pg Os. Iridium was added to Re- and Os-bearing solutions for mass discrimination correction. All uncertainties were determined by error propagation of the uncertainties in the Re and Os mass spectrometer measurements, blank abundances, and spike calibrations. Detailed analytical protocols were described in Qi et al. (2010) and Huang et al. (2013).

4.4. Sulfur and lead isotopic analyses of sulfides

Sulfur isotopes of chalcopyrite, pyrite, and sphalerite minerals were determined at the State Key Laboratory of Environmental Geochemistry (SKLEG), IGCAS (Guiyang), using a Continuous Flow Mass Spectrometer. GBW 04415 ($\delta^{34}S = 22.15‰$) and GBW 04414 ($\delta^{34}S = -0.07‰$) Ag_2S were used as the external standards, and the relative errors (2σ) were better than 0.1‰ from the replication of the standard materials. Sulfur isotopic compositions were reported relative to the Canyon Diablo Troilite (CDT).

Lead isotopic analyses of chalcopyrite, pyrite, and sphalerite minerals were carried out using the GV Isoprobe-T Thermal Ionization Mass Spectrometer at the Beijing Institute of Uranium Geology. The analytical procedure involves dissolution of samples using HF and $HClO_4$ in crucibles, followed by the addition of an anion exchange resin to purify Pb. Analytical results for the standard NBS 981 were $^{208}Pb/^{204}Pb = 36.611 \pm 0.004$ (2σ), $^{207}Pb/^{204}Pb = 15.457 \pm 0.002$ (2σ), and $^{206}Pb/^{204}Pb = 16.937 \pm 0.002$ (2σ), in agreement with the reference values (Belshaw et al., 1998).

4.5. Carbon and oxygen isotopic analyses of calcite grains

C–O isotopic compositions of calcite crystals were obtained using a MAT-251 EM mass spectrometer at the SKLEG. The calcite was reacted with pure phosphoric acid to produce CO_2. The analytical precisions (2σ) were ±0.2‰ for carbon isotopes and ±2‰ for oxygen isotopes. C–O isotopic compositions were reported relative to PDB. $\delta^{18}O_{SMOW} = 1.03086 \times \delta^{18}O_{PDB} + 30.86$ (Friedman and O'Neil, 1977).

Table 3
Re–Os isotopes of pyrites from the Dapingzhang Cu–Pb–Zn ore deposit.

Spot no.	Sample no.	Mineral	Total Re (ppb)	1σ	^{187}Re (ppb)	1σ	^{187}Os (ppb)	1σ	Common Os (ppb)	1σ	$^{187}Re/^{187}Os$	1σ	$^{187}Os/^{187}Os$	1σ	Model age (Ma)	1σ (Ma)
1	DPZ0903	Pyrite	42.3	0.54	26.5	0.34	0.181	0.0025	0.0050	0.0018	40,668	14,735	273	99	411	5.7
2	DPZ0915	Pyrite	18.8	0.32	11.8	0.20	0.076	0.0030	0.0153	0.0011	5900	446	37.1	2.8	385	15
3	DPZ0923	Pyrite	207	5.9	129	3.7	0.830	0.0210	0.4978	0.0067	1997	62.7	12.5	0.21	385	9.7
4	DPZ0924	Pyrite	21.2	0.95	13.3	0.60	0.082	0.0016	0.0435	0.0043	2347	255	14.2	1.4	372	7.2
5	DPZ0928	Pyrite	762	19	477	12	3.392	0.0325	0.0564	0.0079	64,970	9285	452	64	427	4.1
6	DPZ0927	Pyrite	33.0	0.43	20.7	0.27	0.143	0.0016	0.0237	0.0012	6688	343	45.2	2.3	414	4.7
7	DPZ0931	Pyrite	32.6	1.2	20.4	0.73	0.132	0.0033	0.0536	0.0038	2920	233	18.6	1.3	390	9.7
8	DPZ0934	Pyrite	18.8	0.89	11.8	0.55	0.060	0.0014	0.0053	0.0010	17,159	3396	85.6	16	306	7.2

Model ages are calculated using $^{187}Os/^{187}Re = e^{\lambda t} - 1$, where λ ($^{187}Re$ decay constant) $= 1.666 \times 10^{-11}$ a^{-1} with a relative uncertainty of ±0.31% (Smoliar et al., 1996).

4.6. Oxygen and hydrogen isotopic analyses of quartz grains

Hydrogen and oxygen analyses of quartz grains were performed at the Institute of Mineral Resources, Chinese Academy of Geological Science (Beijing), using the Finnigan MAT253 mass spectrometer. Oxygen was liberated from quartz via reaction with BrF_5 (Clayton and Mayeda, 1963) and converted to CO_2 on a platinum-coated carbon rod for oxygen isotope analysis. The water in the fluid inclusions of the quartz was released by heating the samples to above 500 °C using an induction furnace. The water was then reacted with chromium powder at 800 °C to generate hydrogen for isotope analysis (Wan et al., 2005). The results were reported in per mil relative to the V-SMOW standard, with precisions of ±2 per mil (2σ) for δD and ±0.2 per mil (2σ) for $\delta^{18}O$.

5. Analytical results

5.1. Geochemical and Sr–Nd isotopic characteristics of the volcanic rocks

Seventeen quartz- and feldspar–phyric keratophyre and quartz keratophyre samples associated with the Dapingzhang ore deposit were selected for major and trace element analyses (Table 1). The major oxides described below are recalculated to 100% on a volatile-free basis.

The felsic volcanic rock samples in this study from the Dapingzhang ore deposit exhibit high silica (SiO_2 = 72.6–76.3%; volatile-free) and relatively high and variable Al_2O_3 and MgO contents with Al_2O_3 between 12.8 and 14.0% and MgO between 1.84 to 2.82%; however, these samples are poor in most other major elements: TiO_2 = 0.33–0.37%, Fe_2O_3 = 3.28–4.75%, CaO = 0.16–1.1%, MnO = 0.07–0.12%, and P_2O_5 = 0.06–0.07% (Table 1 and Fig. 6). With increasing SiO_2 content, the MgO, TiO_2, Fe_2O_3, Al_2O_3, and P_2O_5 contents slightly decrease (Fig. 6).

On the ($Na_2O + K_2O$) vs. SiO_2 diagram (Fig. 7a; Irvine and Baragar, 1971; Le Bas and Streckeisen, 1991), the volcanic rocks are plotted mainly in the subalkaline rhyolite field with minor basaltic, andesitic and dacitic rocks. Meanwhile, the volcanic rock samples have relatively low K_2O concentrations. On the K_2O vs. SiO_2 diagram (Fig. 7b; Rickwood, 1989), the volcanic rocks exhibit the affinities of calc-alkaline volcanic rocks.

The studied volcanic rocks show low total REE contents (28.8–87.3 ppm), slightly to moderately LREE-enriched (La_N = 11–49, $(La/Yb)_N$ = 1.0–3.8; $(La/Sm)_N$ = 1.7–2.5) and slightly HREE-humped ($(Gd/Yb)_N$ = 0.5–1.1) patterns, with slightly to distinctly negative Eu anomalies (Eu/Eu^* = 0.48–0.89) (Fig. 8a). All of the samples exhibit obviously negative anomalies of Nb, Ta, and Sr in the primitive mantle-normalized multi-element plot (Sun and McDonough, 1989) (Fig. 8b).

Nd and Sr isotopes for the representative volcanic rocks associated with the Dapingzhang ore deposit are listed in Table 2. They display limited variations in $^{143}Nd/^{144}Nd$ ratios from 0.512718 to 0.512841, corresponding to initial $\varepsilon_{Nd}(t)$ values of +4.4 to +6.5. These samples have slightly variable $^{87}Sr/^{86}Sr$ (0.708817–0.709804) ratios, corresponding to age-corrected $(^{87}Sr/^{86}Sr)_i$ ratios from 0.7050 to 0.7076 (Table 2; Fig. 9).

5.2. Re–Os ages of pyrites

Eight pyrite samples from the Dapingzhang Cu–Pb–Zn ore deposit were selected for Re–Os isotopic analyses (Table 3). These samples have ~18.8 to 762 ppb Re, 11.8 to 477 ppb ^{187}Re, and 0.060 and 3.39 to ^{187}Os. However, their common Os and radiogenic ^{187}Os contents range from 0.005 to 0.498 ppb and from 0.060 to 3.39 ppb, respectively. The extremely high $^{187}Re/^{188}Os$ values (~1997 to 64,970) and highly radiogenic $^{187}Os/^{188}Os$ ratios (~12.5 to 452) of these samples identify them as "LLHR" (low-level highly radiogenic) sulfides as defined by Stein et al. (2000).

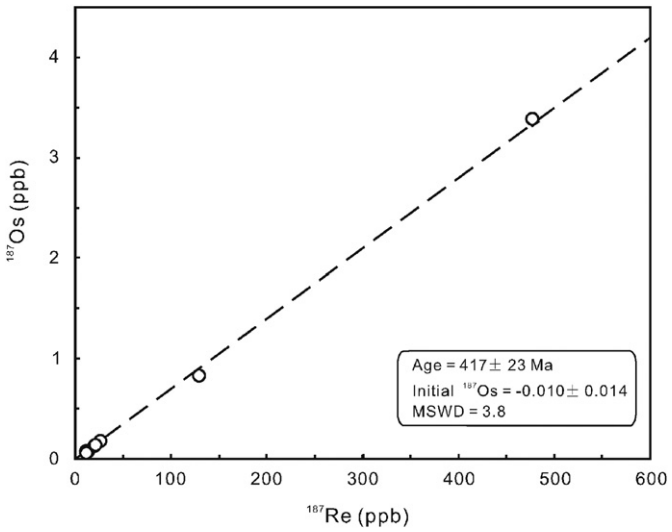

Fig. 10. ^{187}Re versus ^{187}Os plot of pyrite separates from the Dapingzhang Cu–Pb–Zn ore deposit. The isochron age was calculated using Isoplot/Ex version 3.23. Ludwig (2003).

As the low ^{188}Os contents cannot be determined precisely due to the blank correction, traditional $^{187}Re/^{188}Os$ and $^{187}Os/^{188}Os$ plots for "LLHR" sulfides would introduce large uncertainties. Using the ^{187}Re vs. ^{187}Os plot instead of the traditional $^{187}Re/^{188}Os$ vs. $^{187}Os/^{188}Os$ plot can avoid large analytical uncertainties and highly correlated errors (Stein et al., 2000). All eight samples define a ^{187}Re vs. ^{187}Os isochron age of 417 ± 23 Ma (MSWD = 3.8) (Fig. 10), which is the best estimate of the ore-forming age of the Dapingzhang deposit.

Table 4
Sulfur isotopic compositions of sulfide minerals from the Dapingzhang Cu–Pb–Zn ore deposit.

Spot No.	Sample No.	Ore type	Mineral	$\delta^{34}S_{V\text{-}CDT}$ (‰)
1	DPZ0901	Disseminated sulfide ore	Pyrite	1.88
2	DPZ0901	Disseminated sulfide ore	Chalcopyrite	1.84
3	DPZ0902	Disseminated sulfide ore	Chalcopyrite	4.03
4	DPZ0903	Disseminated sulfide ore	Pyrite	1.86
5	DPZ0905	Disseminated sulfide ore	Pyrite	4.32
6	DPZ0905	Disseminated sulfide ore	Chalcopyrite	3.69
7	DPZ0907	Massive sulfide ore	Chalcopyrite	−1.04
8	DPZ0908	Massive sulfide ore	Chalcopyrite	0.88
9	DPZ0909	Massive sulfide ore	Chalcopyrite	2.98
10	DPZ0910	Massive sulfide ore	Chalcopyrite	2.64
11	DPZ0913	Massive sulfide ore	Pyrite	1.26
12	DPZ0913	Massive sulfide ore	Chalcopyrite	0.51
13	DPZ0914	Massive sulfide ore	Chalcopyrite	2.92
14	DPZ0915	Massive sulfide ore	Pyrite	1.40
15	DPZ0916	Massive sulfide ore	Pyrite	2.50
16	DPZ0918	Massive sulfide ore	Chalcopyrite	−0.95
17	DPZ0919	Massive sulfide ore	Chalcopyrite	0.10
18	DPZ0921	Massive sulfide ore	Chalcopyrite	−0.02
19	DPZ0922	Massive sulfide ore	Chalcopyrite	−0.05
20	DPZ0923	Massive sulfide ore	Pyrite	−1.24
21	DPZ0924	Massive sulfide ore	Pyrite	1.31
22	DPZ0925	Massive sulfide ore	Pyrite	2.35
23	DPZ0927	Massive sulfide ore	Pyrite	1.48
24	DPZ0928	Massive sulfide ore	Chalcopyrite	−0.05
25	DPZ0930	Massive sulfide ore	Chalcopyrite	−0.01
26	DPZ0931	Massive sulfide ore	Pyrite	0.97
27	DPZ0931	Massive sulfide ore	Chalcopyrite,	−0.21
28	DPZ0934	Massive sulfide ore	Pyrite	0.90
29	DPZ0936	Massive sulfide ore	Chalcopyrite,	1.54
30	DPZ0937	Massive sulfide ore	Sphalerite	0.96
31	DPZ0938	Massive sulfide ore	Pyrite	2.25

Note: Analytical uncertainty is 2σ.

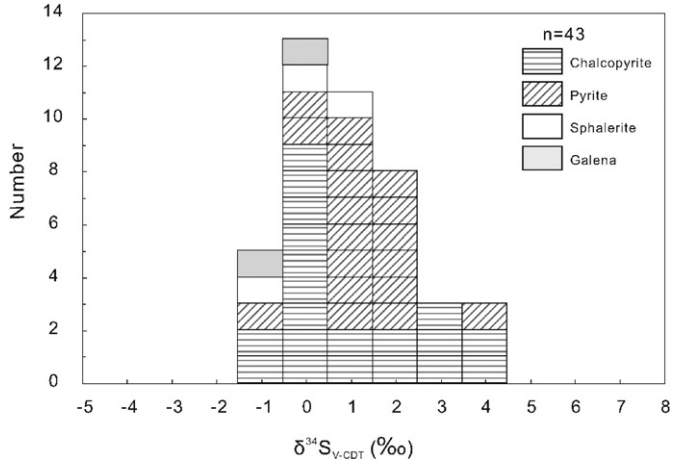

Fig. 11. Histogram of the sulfur isotopic compositions of sulfide minerals from the Dapingzhang Cu–Pb–Zn ore deposit.
The other S isotopic data are from Zhong et al. (2000).

5.3. S–Pb isotopic compositions of sulfides

The sulfur isotopic compositions of the sulfide minerals from the Dapingzhang ore deposit are listed in Table 4. In the histogram, chalcopyrite and pyrite display slightly variable $\delta^{34}S_{CDT}$ values, whereas sphalerite and galena exhibit fairly constant values (Fig. 11). The $\delta^{34}S_{CDT}$ values for chalcopyrite, pyrite, sphalerite, and galena minerals range from −1.04 to +4.03‰, −1.24 to +4.32‰, −1.05 to +0.96‰, and −0.51 to −0.50‰, respectively. The relatively homogeneous sulfur isotopic compositions indicate a consistent sulfur source for the Dapingzhang deposit.

Pb isotopic compositions of sulfide minerals from the Dapingzhang ore deposit are listed in Table 5. Sulfide minerals have relatively homogeneous and characteristically low radiogenic Pb isotopic compositions with $^{206}Pb/^{204}Pb$ ranging from 18.310 to 18.656, $^{207}Pb/^{204}Pb$ from 15.489 to 15.643, and $^{208}Pb/^{204}Pb$ from 37.811 to 38.662. The ore-hosting volcanic rocks display similar $^{206}Pb/^{204}Pb$ ratios (17.910–18.850), $^{207}Pb/^{204}Pb$ (15.547–15.619), and $^{208}Pb/^{204}Pb$ (37.987–38.714) ratios (Table 5). In the plumbotectonic diagram of Zartman and Doe (1981), the Pb-isotopic data of the sulfide samples are plotted between the boundary of the mantle and upper crustal reservoirs (Fig. 12a and b).

5.4. C–O isotopic compositions of calcite crystals

C and O isotopic analyses of calcite grains from the massive ores of the Dapingzhang ore deposit are listed in Table 6. These hydrothermal calcite separates have relatively uniform C and O isotopic compositions with $\delta^{13}C_{PDB}$ values ranging from −2.3 to +0.27‰, $\delta^{18}O_{PDB}$ values ranging from −15.8 to −6.3‰, and $\delta^{18}O_{SMOW}$ values ranging from +14.6 to +24.4‰ (Table 6; Fig. 13).

5.5. H and O isotopic compositions of quartz separates

New oxygen and hydrogen isotopic compositions of 10 quartz separates of the Dapingzhang Cu–Pb–Zn ore deposit are listed in Table 7. The $\delta^{18}O$ values of the quartz grains range from +8.2 to +10.4‰ for the disseminated ores and from +7.8 to +10.5‰ for the massive ores, respectively. The hydrogen isotopic compositions analyzed directly on fluid inclusions gave a relatively narrow spread between −72‰ and −92‰ for the disseminated ores and between −59‰ and −84‰ for the massive ores (Fig. 14).

6. Discussion

6.1. Timing of Cu–Pb–Zn mineralization

We obtained the first reliable pyrite Re–Os isotopic isochron age of 417 ± 23 Ma (Fig. 10), which is indistinguishable (within the analytical uncertainty) from the Re–Os dating of 429 ± 10 Ma for the bulk-ore samples and the LA-ICP-MS zircon U–Pb dating of 429 ± 2 Ma for the associated felsic rocks from the Dapingzhang Cu–Pb–Zn ore deposit (Lehmann et al., 2013). In addition, the Dazhonghe basaltic andesite to andesite in this area (Fig. 2) have also been dated at 421–417 Ma (Mao et al., 2012). The above ages demonstrate that the Cu–Pb–Zn mineralization at Dapingzhang occurred during the mid-Silurian (ca. 430–420 Ma), which is consistent with the formation of the ore-hosting felsic volcanic rocks and the Dazhonghe andesitic volcanic rocks.

6.2. The petrogenesis of the Dapingzhang volcanic rocks

The compositional variations of the Dapingzhang volcanic rocks imply various degrees of fractional crystallization (Fig. 6). The Dapingzhang felsic volcanic rocks show a distinct decrease of the MgO and Fe_2O_3 contents with increasing SiO_2 contents (Table 1 and Fig. 6), which is interpreted as being due to the fractionation of MgO- and Fe_2O_3-rich minerals such as hornblende. From the REE patterns, hornblende may be considered an important phase fractionated from magmas because it is able to produce a fairly flat HREE pattern without significant HREE fractionation in intermediate and acidic magmas (Martin et al., 1994; Han et al., 1997). Therefore, the presence of Eu and Sr negative anomalies in the felsic volcanic rocks are indicative of fractionation of plagioclase (Wu et al., 2002). The negative correlation of TiO_2 with SiO_2 in the rocks is commonly related to ilmenite or titanite fractionation (Fig. 6). In addition, P_2O_5 contents decrease with increasing SiO_2, showing apatite fractionation (Fig. 6). The felsic samples with relatively low REE contents were most likely due to more apatite fractionation and consequent depletion of REE in the melt (Table 1 and Fig. 8; Watson and Capobianco, 1981). As a result, these chemical

Table 5
Lead isotopic compositions of sulfide minerals from the Dapingzhang Cu–Pb–Zn ore deposit.

Spot no.	Sample no.	Ore type	Mineral	$^{206}Pb/^{204}Pb$ (2σ)	$^{207}Pb/^{204}Pb$ (2σ)	$^{208}Pb/^{204}Pb$ (2σ)
1	DPZH0901	Disseminated sulfide ore	Pyrite	18.382 ± 0.003	15.541 ± 0.002	38.139 ± 0.005
2	DPZH0902	Disseminated sulfide ore	Chalcopyrite	18.656 ± 0.002	15.643 ± 0.002	38.662 ± 0.005
3	DPZH0905	Disseminated sulfide ore	Pyrite	18.547 ± 0.004	15.635 ± 0.003	38.402 ± 0.008
4	DPZH0905	Disseminated sulfide ore	Chalcopyrite	18.645 ± 0.004	15.615 ± 0.003	38.610 ± 0.008
5	DPZH0915	Massive sulfide ore	Pyrite	18.414 ± 0.003	15.545 ± 0.002	38.013 ± 0.006
6	DPZH0923	Massive sulfide ore	Pyrite	18.427 ± 0.004	15.550 ± 0.003	38.092 ± 0.008
7	DPZH0925	Massive sulfide ore	Pyrite	18.362 ± 0.004	15.558 ± 0.003	38.194 ± 0.008
8	DPZH0928	Massive sulfide ore	Chalcopyrite	18.456 ± 0.002	15.533 ± 0.002	37.957 ± 0.005
9	DPZH0937	Massive sulfide ore	Chalcopyrite	18.375 ± 0.002	15.522 ± 0.002	37.984 ± 0.004
10	DPZH0938	Massive sulfide ore	Pyrite	18.477 ± 0.004	15.640 ± 0.003	38.427 ± 0.008

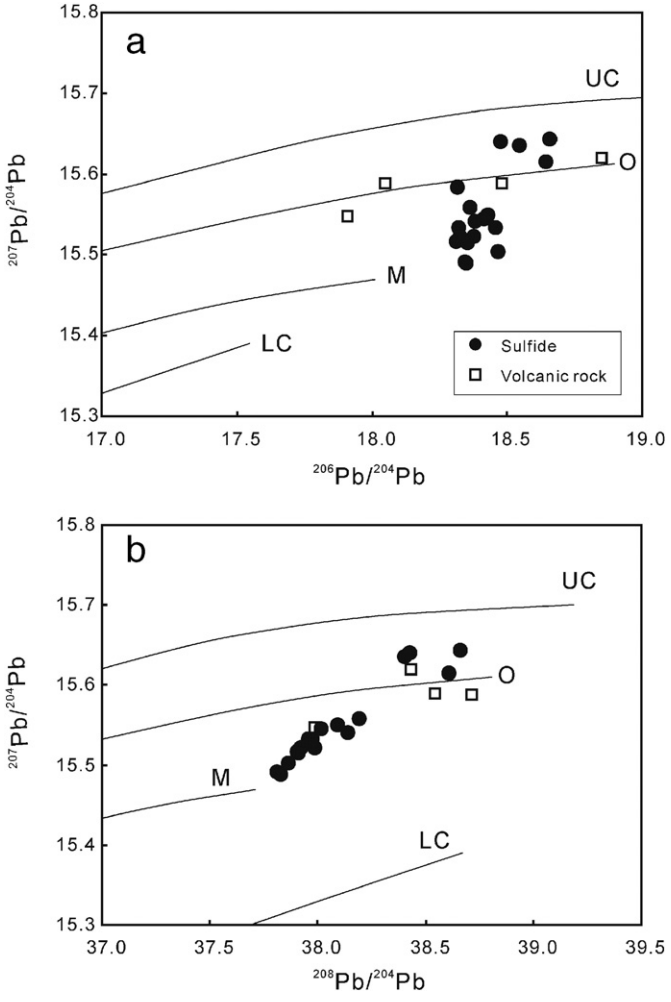

Fig. 12. $^{207}Pb/^{204}Pb$ vs. $^{206}Pb/^{204}Pb$ diagram (a) and $^{207}Pb/^{204}Pb$ vs. $^{208}Pb/^{204}Pb$ diagram (b) of sulfides and ore-hosting volcanic rocks from the Dapingzhang Cu–Pb–Zn ore deposit. Lead isotopic curves for the upper crust, lower crust, orogen, and mantle are from Zartman and Doe (1981).
The other Pb isotopic data are from Zhong et al. (2000).

variations for the Dapingzhang felsic volcanic rocks are consistent with the extensive crystal fractionation of ferromagnesian minerals, plagioclase, and minor Fe–Ti oxides and apatite.

The Dapingzhang felsic rocks display relatively low Nb and Y contents, similar to those of I-type volcanic arc rocks (Fig. 15a). Several genetic models have been proposed to account for the origin and petrogenesis of the felsic arc magmas. The mechanisms include (1) products of fractional crystallization or AFC of mantle-derived basaltic magmas (e.g., Grove and Donnelly-Nolan, 1986; Eggins and Hensen, 1987; Bacon and Druitt, 1988), (2) partial melting of juvenile sub-alkaline metabasaltic rocks (e.g., Drummond and Defant, 1990; Rushmer, 1991; Rapp and Watson, 1995), and (3) partial melting of crustal rocks due to underplating of basaltic magmas (e.g., Bullen and Clynne, 1990; Tepper et al., 1993; Guffanti et al., 1996).

All of the Dapingzhang volcanic rocks are characterized by depleted mantle-like Nd isotopic compositions ($\varepsilon_{Nd}(t) = 4.4–6.5$), indicating minimal involvement of ancient continental components (Fig. 9). The MgO vs. SiO_2 plot (Fig. 15b) shows the experimental liquids obtained from the melting of basaltic protoliths. At a given SiO_2 content, these felsic rocks have MgO contents obviously higher than the experimental melts, indicating that it is unlikely that they were generated by melting of the juvenile metabasaltic rocks. Thus, the above features suggest that the Dapingzhang felsic volcanic rocks were possibly formed by crystal fractionation of coeval mantle-derived mafic magmas.

The Dapingzhang felsic rock samples display consistent Nd isotopic compositions with the spilite in the deposit ($\varepsilon_{Nd}(t) = 5.4$; Lehmann et al., 2013) and the coeval Dazhonghe basaltic andesite to andesitic rocks in this area ($\varepsilon_{Nd}(t) = 3.9–4.4$; Mao et al., 2012). However, they have higher SiO_2 contents and lower total REE contents and $(La/Yb)_N$ ratios than those of the Dazhonghe andesitic volcanic rocks (Mao et al., 2012), which is not consistent with the fractional crystallization process of a common magma. It is therefore suggested that the magma parents of the Dapingzhang and Dazhonghe volcanic rocks were unlikely to be derived from a common basaltic melt by fractional crystallization.

In contrast, the Dapingzhang felsic volcanic rocks were possibly products of fractional crystallization of mantle-derived basaltic magma parents of the associated spilites. The spilites exhibit higher MgO, TiO_2, Fe_2O_3, Al_2O_3, and P_2O_5 contents and lower total REE contents (Figs. 6 and 8). In addition, the spilites are characterized by negative anomalies of Nb, Ta, and consistent REE and trace element patterns, which is similar to those of the felsic volcanic rocks (Fig 8). Thus, the felsic volcanic rocks were generated by extensive fractional crystallization of the resulting basaltic magma parents of the Dapingzhang spilites during emplacement.

Zircon U–Pb dating results indicate that the Nantinghe ophiolites were formed 444–439 Ma (Wang et al., 2013), implying that the Paleo-Tethys Ocean basin at least existed during the early Paleozoic in the Changning–Menglian zone. In addition, previous studies show that the Dazhonghe volcanic rocks are similar to the features of the island arc rocks within the continental margin (Mao et al., 2012). Therefore, the generation of the Dapingzhang volcanic rocks is most likely associated with the mid-Silurian eastward subduction of the Paleo-Tethys Ocean. A likely scenario of the petrological process can be described as follows: The eastward subduction of the Changning–Menglian oceanic plate resulted in partial melting associated with metasomatism of the depleted mantle wedge over the subducted slab. The resulting basaltic magmas were similar to the compositions of the magma parents of the Dapingzhang spilites. The basaltic magmas would be continuously injected into the shallow-level chamber and extensive fractional crystallization could be responsible for the formation of the Dapingzhang felsic volcanic rocks.

6.3. Possible sources of ore metals

In the Dapingzhang deposit, chalcopyrite, pyrite, galena, and chalcopyrite are the dominant ore minerals. The lack of sulfate minerals in the ores suggests that the $\delta^{34}S$ values of the sulfides could basically represent the total S isotopic composition of the hydrothermal fluid, i.e., $\delta^{34}S$ (sulfide) $\approx \delta^{34}S$ (fluid) (Ohmoto, 1972; Kelly and Rye, 1979). Therefore, these values can be used directly to represent the sulfur

Table 6
C and O isotopic compositions of calcite crystals from the Dapingzhang Cu–Pb–Zn ore deposit.

Spot No.	Sample	Ore type	Mineral	$\delta^{13}C_{PDB}$ (‰)	$\delta^{18}O_{PDB}$ (‰)	$\delta^{18}O_{SMOW}$ (‰)
1	DPZH0911	Massive sulfide ore	Calcite	−0.10	−15.8	14.6
2	DPZH0915	Massive sulfide ore	Calcite	−2.30	−15.6	14.8
3	DPZH0923	Massive sulfide ore	Calcite	−0.16	−14.4	16.0
4	DPZH0925	Massive sulfide ore	Calcite	−1.07	−10.1	20.5
5	DPZH0932	Massive sulfide ore	Calcite	0.27	−6.29	24.4

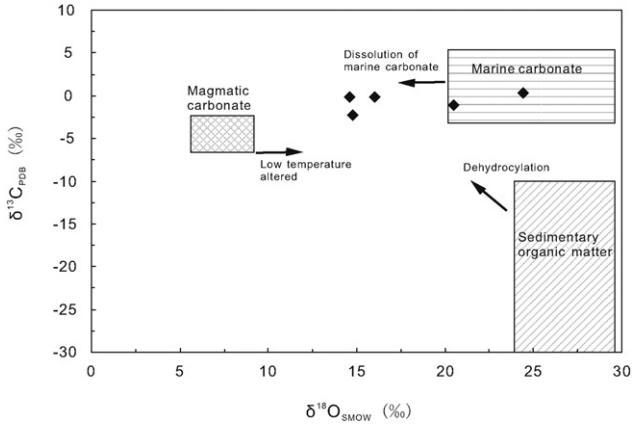

Fig. 13. $\delta^{13}C_{PDB}$ vs. $\delta^{18}O_{SMOW}$ plot for the Dapingzhang Cu–Pb–Zn ore deposit. Fields for magmatic, marine carbonates, and sedimentary organic matter are from Ohmoto (1986) and Vezier and Hoefs (1976), respectively.

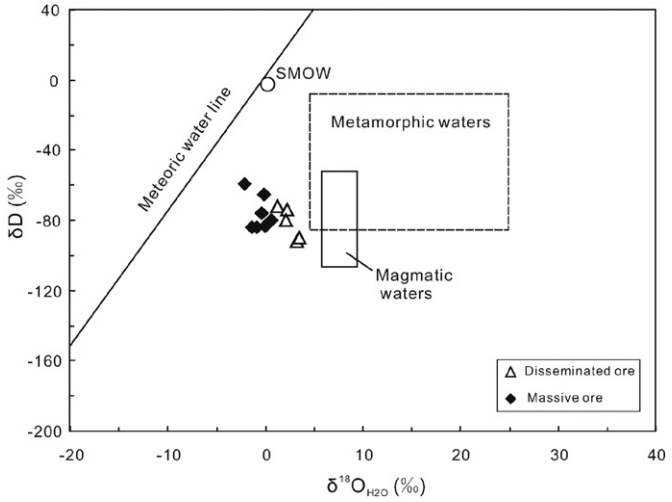

Fig. 14. Hydrogen versus oxygen isotope diagram showing the compositions of hydrothermal fluids for ore-bearing quartz grains from the Dapingzhang ore deposit. Meteoric water line and primary magmatic water box are taken from Taylor (1979). The other H–O isotopic data are from Zhong et al. (2000).

source. The $\delta^{34}S$ values are restricted to the interval of −1.2‰ to +4.3‰ (average + 1.0‰; Table 4 and Fig. 11). Traditionally, a $\delta^{34}S$ value of approximately 0‰ is taken to indicate a magmatic fluid (Chaussidon et al., 1989). The relatively narrow range of $\delta^{34}S$ values for the sulfides from the Dapingzhang ore deposit indicates that the sulfur in the ores was mainly derived from a magmatic source with a minor crustal contribution. The sulfur of igneous origin was either leached from the spatially and temporally associated volcanic rocks or directly derived from magmatic fluids.

As shown from the plumbotectonic diagram (Fig. 12) of Zartman and Doe (1981), the Pb-isotopic data of the sulfide samples are plotted over a relatively narrow range from the mantle, orogenic, to upper crustal reservoirs. The data on the sulfide samples present a relatively good linear correlation, which probably indicates the mixing of more mantle lead with small amounts of upper crust lead. The data of the volcanic rocks from the Longdonghe Formation (S_2l) are plotted near the orogen reservoir (Fig. 12). The plot clearly shows no differences between the sulfide minerals and the volcanic rocks, indicating that they share the same lead source. The Pb isotopic data of the Dapingzhang sulfide minerals and ore-hosting volcanic rocks suggest a mixed source of primarily primitive mantle-type Pb and small amounts of radiogenic crustal Pb.

The above S–Pb isotopic compositions indicate that S, Pb, and probably the other metals (Cu and Zn) were primarily derived from the spatially and temporally associated felsic volcanic rocks at Dapingzhang. The minor radiogenic Pb suggests that subordinate ore-forming metals originated from the underlying basement rocks.

6.4. Origin of the hydrothermal fluids

In the diagram of $\delta^{13}C_{PDB}$ vs. $\delta^{18}O_{SMOW}$ (Fig. 13), all calcite crystals are plotted in the field between the mantle and marine carbonate and close to marine carbonate rocks. If the CO_2 in hydrothermal fluids was derived from the mantle, precipitated hydrothermal calcite would show constant $\delta^{13}C$ with high $\delta^{18}O$ values (Demény et al., 1998). Similarly, if CO_2 originated from marine carbonate rocks, precipitated hydrothermal calcite would display constant $\delta^{13}C_{PDB}$ with low $\delta^{18}O_{SMOW}$ values (Demény and Harangi, 1996). Therefore, the constant $\delta^{13}C$ and high $\delta^{18}O$ values of the calcite grains indicate that the CO_2 in the hydrothermal fluids was primarily derived from marine carbonates (Fig. 13).

The $\delta^{18}O_{H_2O}$ values were calculated from the $\delta^{18}O$ values for quartz and fluid inclusion homogenization temperatures in quartz using the equation for quartz–water isotopic equilibrium (Matsuhisa et al., 1979). The highest homogenization temperatures of the fluid inclusions are ca. 300 °C and 230 °C in quartz grains from the disseminated ores and the massive ores, respectively (Li et al., 2000). The hydrothermal fluids that precipitated quartz yield a range of $\delta^{18}O_{H_2O}$ values from +1.3 to +3.5‰ for the disseminated ores and from −2.1 to +0.61‰ for the massive ores (Table 7). In a plot of δD vs. $\delta^{18}O_{H_2O}$ (Fig. 14), the $\delta^{18}O_{H_2O}$ and δD_{H_2O} values are plotted in the area between the magmatic domain and the meteoric water

Table 7
Hydrogen and oxygen isotopic compositions of quartz grains from the Dapingzhang Cu–Pb–Zn ore deposit.
The equation for quartz–water isotopic equilibrium ($1000\ln\alpha_{Quartz\text{-}H_2O} = \delta^{18}O_{Quartz} - \delta^{18}O_{H_2O} = 3.34\times10^6\ T^{-2} - 3.31$) is from Matsuhisa et al. (1979).

Spot no.	Sample no.	Ore type	Mineral or rock	$\delta D_{V\text{-}SMOW}$ (‰)	$\delta^{18}O_{V\text{-}SMOW}$ (‰)	$\delta^{18}O_{H_2O}$ (‰) (300 °C)	$\delta^{18}O_{H_2O}$ (‰) (230 °C)
1	DPZH0901	Disseminated sulfide ore	Quartz	−72	8.2	1.3	
2	DPZH0902	Disseminated sulfide ore	Quartz	−92	10.2	3.3	
3	DPZH0903	Disseminated sulfide ore	Quartz	−90	10.4	3.5	
4	DPZH0905	Disseminated sulfide ore	Quartz	−74	9.2	2.3	
5	DPZH0906	Disseminated sulfide ore	Quartz	−80	9.0	2.1	
6	DPZH0909	Massive sulfide ore	Quartz	−84	9.1		−0.79
7	DPZH0910	Massive sulfide ore	Quartz	−84	8.6		−1.3
8	DPZH0913	Massive sulfide ore	Quartz	−80	10.5		0.61
9	DPZH0914	Massive sulfide ore	Quartz	−76	9.5		−0.39
10	DPZH0934	Massive sulfide ore	Quartz	−83	9.9		0.01

SMOW—standard mean ocean water.

line, close to the magmatic water area. According to the C–O isotopic data of calcite grains, the water was likely from the sea.

From the above discussions, the field geology and C–O isotopic data of calcite crystals from the massive ores indicate that the massive ores were most likely formed at or near the seafloor. The Dapingzhang ore-forming hydrothermal fluids consist of magmatic fluid and seawater. From the disseminated ores to the massive ores, the H–O isotopic data may reflect the progressively increasing influence of the seawater contribution during the evolution of the ore-forming fluids.

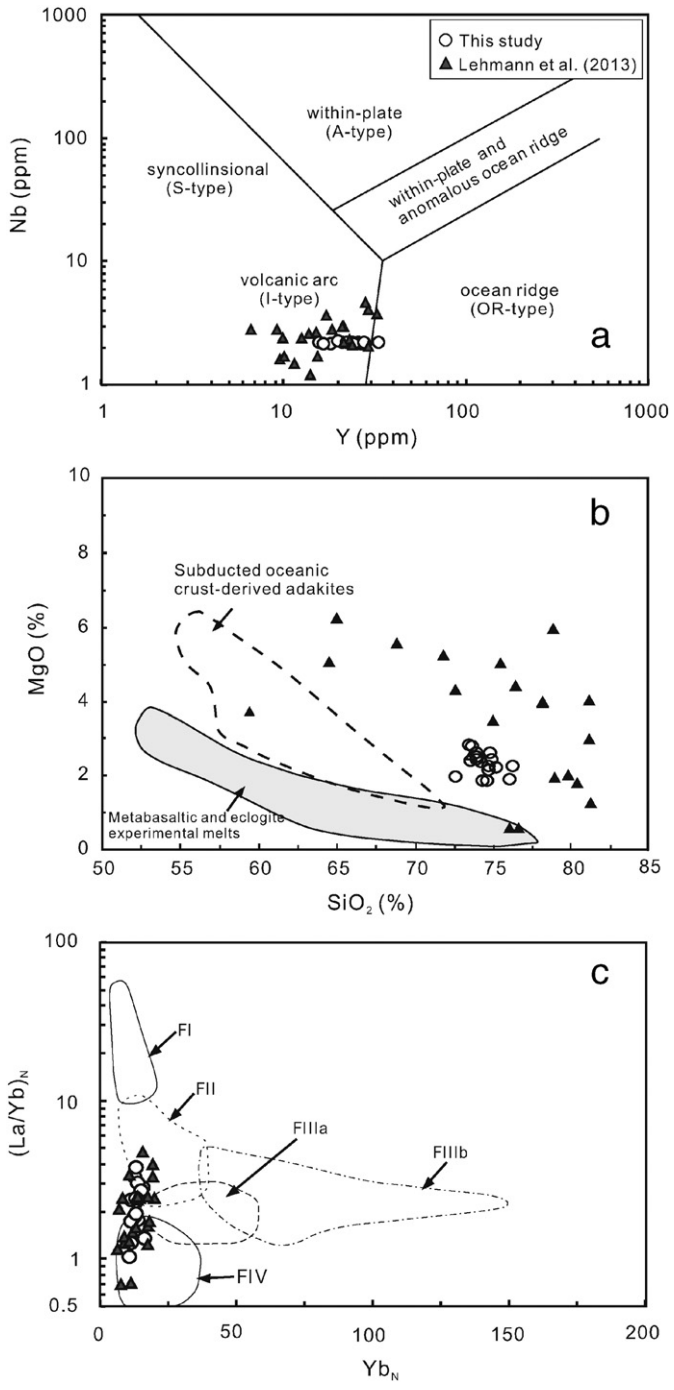

Fig. 15. (a) Nb vs. Y tectonic discrimination diagram after Pearce et al. (1984), (b) MgO vs. SiO_2 diagram from Li et al. (2009), and (c) $(La/Yb)_N$ vs. Yb_N diagram with field subdivisions from Hart et al. (2004) for the felsic volcanic rocks from the Dapingzhang Cu–Pb–Zn ore deposit.

6.5. Implications for ore-forming processes

Well-defined volcanic breccia pipes with few stockwork and abundant disseminated sulfide ores are recorded below the stratiform massive sulfide ores in the Dapingzhang deposits (see Fig. 4a and b). The altered volcaniclastic rocks most likely represent the altered products of a deeper feeder system through which the hydrothermal fluids discharged. Our new geochronologic, multiple isotopic (S, Pb, H, O, C), and geochemical data in this study provide further constraints on the timing and genesis of the Dapingzhang ores. The age of the Cu–Pb–Zn mineralization at Dapingzhang is consistent with the age of the ore-hosting volcanic rocks, which are characterized by arc-related felsic rocks. The S–Pb isotopic data also show that the ore-forming metals (Cu–Pb–Zn) originated from arc-related felsic rocks. The felsic rocks from the deposit display variably and relatively low Cu (2.48–230 ppm, mostly <10 ppm), Zn (41.7–162 ppm, mostly <90 ppm), and Pb (1.04–6.69 ppm, mostly <3.50 ppm) contents (Table 1). Thus, Cu, Zn and Pb could have been leached from the felsic volcanic rocks by convective hydrothermal fluids to form the Dapingzhang ore deposit. The H–O isotopic data of quartz grains indicate that the fluids changed from a significant magmatic contribution to the evolved seawater-dominated convective hydrothermal system. To explain the anomalous Cu–Pb–Zn content, the magmatic contribution of Cu–Pb–Zn is consistent with the magmatic fluid sources. Therefore, the Cu–Pb–Zn mineralization at Dapingzhang is genetically and spatially associated with the felsic volcanic rocks. The sources of the ore-forming hydrothermal fluids and metals suggest that the Dapingzhang Cu–Pb–Zn deposit is a typical volcanic-hosted massive sulfide deposit.

In the Dapingzhang area, we envision a genetic model in which ca. 430–420 Ma magmatism provided S-bearing magmatic fluids and heat that promoted convective circulation of seawater, and metals leached from ca. 430–420 Ma volcanic rocks. For the disseminated style mineralization, the H_2S that was exolved from the magma reacted with Fe-bearing minerals from igneous wall rocks to produce the disseminated ore minerals. This suggests lithological and alteration control, as observed within the Dapingzhang Cu–Pb–Zn disseminated sulfide ores formed above the altered rhyolitic rocks (see Fig. 4a and b). In addition, the magmatic fluids likely mixed with various amounts of seawater, which promoted the precipitation of Cu–Pb–Zn sulfides to form the ores. However, mineralogical textures in the Dapingzhang deposit suggest that the massive sulfide ores formed mainly on or near the seafloor. Therefore, the hot magmatic-dominated fluids mixed with more seawater to form the mound for the massive mineralization.

Volcanogenic massive Cu–Zn–(Pb) sulfide (VMS) deposits occur primarily in subaqueous rift-related environments (e.g., oceanic, fore-arc, arc, back-arc, continental margin, or continental) (Hart et al., 2004). On the $(La/Yb)_N$ vs. Yb diagram (Fig. 15c; Hart et al., 2004; Bissig et al., 2008), the calc-alkaline felsic volcanic rocks at Dapingzhang mainly exhibit affinities with FII and FIV fields. In most cases, volcanogenic massive Cu–Zn–Pb deposits associated with the FII- and FIV-type volcanic rocks usually formed in rifted continental arc or continental back-arc environments (Hart et al., 2004; Bissig et al., 2008). Therefore, it is conceivable that the Dapingzhang volcanic rocks were formed in a rifted island arc environment within the continental margin that was associated with the mid-Silurian eastward subduction of the Paleo-Tethys Ocean.

7. Conclusions

(1) The new Re–Os pyrite age shows that sulfide mineralization in the Dapingzhang volcanogenic Cu–Pb–Zn ore deposit occurred 417 ± 23 Ma, consistent with previous results from Re–Os isotopic analyses of ore samples from the deposit. This study indicates that the timing of the sulfide mineralization at Dapingzhang is similar to the U–Pb age of comagmatic zircon crystals from felsic volcanic rocks in the region.

(2) It is suggested that the felsic volcanic rocks associated with the Dapingzhang deposit formed by extensively fractionated magma from a basaltic magma in a rifted island arc setting.
(3) The S isotopic compositions of sulfide minerals from the deposit indicate a predominant magmatic source for the sulfur. The Pb isotopic compositions of the host volcanic rocks and sulfide minerals from the deposit are similar, suggesting that the Pb in the sulfide ores and volcanic rocks share a common source.
(4) The C–O isotopes of calcite and the H–O isotopes of quartz from the deposit indicate mixing between magmatic fluids and heated seawater in the Dapingzhang ore-forming hydrothermal system.
(5) The most important exploration implication from the established genetic relationship between the Dapingzhang Cu–Pb–Zn ore deposit is that the mid-Silurian volcanic belt has potential for new discoveries of more volcanogenic base metal sulfide deposits.

Acknowledgments

This study was financially supported by the National Basic Research Program of China (2009CB421003), the CAS/SAFEA International Partnership Program for Creative Research Teams (Intraplate Mineralization Research Team; KZZD-EW-TZ-20), the National Natural Science Foundation of China (Grants 41273049), and the State Key Laboratory of Ore Deposit Geochemistry (12th Five-Year Plan: SKLOG-ZY125-06). This paper has benefited greatly from the very detailed and constructive comments by C. Li, the editor and the two anonymous reviewers. We thank G.H. Yin, D.F. He and H.P. Fan for their field assistance, Y.F. Yin for the assistance in Re–Os isotopic analyses, N. An for the assistance in S and C–O isotopic analyses, Y.H. Li for the assistance in H–O isotopic analyses, Y.X. Hou for the assistance in Pb isotopic analyses, J. Hu, Y. Huang and G.P. Bao for whole-rock trace element analyses by ICP-MS, and F. Xiao and B.L. Huang for Sr–Nd isotopic analyses by MC-ICP-MS.

References

Bacon, C.R., Druitt, T.H., 1988. Compositional Evolution of the Zoned Calcalkaline Magma Chamber of Mount-Mazama, Crater Lake. Oregon. Contrib. Mineral. Petrol. 98, 224–256.
Belshaw, N.S., Freedman, P.A., O'Nions, R.K., Frank, M., Guo, Y., 1998. A new variable dispersion double-focusing plasma mass spectrometer with performance illustrated for Pb isotopes. Int. J. Mass Spectrom. 181, 51–58.
Bissig, T., Mortensen, J.K., Tosdal, R.M., 2008. The rhyolite-hosted volcanogenic massive sulfide district of Cuale, Guerrero terrane, west-central Mexico: silver-rich, base metal mineralization emplaced in a shallow marine continental margin setting. Econ. Geol. 103, 141–159.
Boynton, W.V., 1984. Geochemistry of the Rare Earth Elements: Meteorite Studies. In: Henderson, P. (Ed.), Rare Earth Element Geochemistry. Elsevier, pp. 63–114.
Bullen, T.D., Clynne, M.A., 1990. Trace element and isotopic constraints on magmatic evolution at Lassen Volcanic Center. J. Geophys. Res. 95, 19671–19691.
Chaussidon, M., Albarède, F., Sheppard, S.M.F., 1989. Sulphur isotope variations in the mantle from ion microprobe analyses of micro-sulphide inclusions. Earth Planet. Sci. Lett. 92, 144–156.
Chen, L., Wang, L.Q., Wang, B.D., Liu, H., 2013. Genesis of Guanfang copper deposit in the Yunxian-Jinggu volcanic arc, western Yunnan: evidences from fluid inclusions and geochronology. Acta Pet. Sin. 29, 1279–1289 (in Chinese with English abstract).
Chen, Y.L., Luo, Z.H., Liu, C., 2001. New recognition of Kangding–Mianning metamorphic complexes from Sichuan, western Yangtze Craton. Earth Sci. J. China Univ. Geosci. 26, 279–285.
Clayton, R.N., Mayeda, T.K., 1963. The use of bromine pentafluoride in the extraction of oxygen from oxides and silicates for isotopic analysis. Geochim. Cosmochim. Acta 27, 43–52.
Dai, B.Z., Liao, Q.L., Jiang, S.Y., 2004. Isotope geochemistry and mineralization age of the Dapingzhang copper-polymetallic deposit in Lanping-Simao basin, Yunnan province. J. Nanjing Univ. (Nat. Sci.) 40, 674–683 (in Chinese with English abstract).
Demény, A., Harangi, S.Z., 1996. Stable isotope studies on carbonate formations in alkaline basalt and lamprophyre series: evolution of magmatic fluids and magmasediment interactions. Lithos 37, 335–349.
Demény, A., Ahijado, A., Casillas, R., Vennemann, T.W., 1998. Crustal contamination and fluid/rock interaction in the carbonatites of Fuerteventura (Canary Islands, Spain): a C, O, H isotope study. Lithos 44, 101–115.
Drummond, M.S., Defant, M.J., 1990. A modal for trondhjemite–tonalite–dacite genesis and crustal growth via slab melting: Archaean to modern comparisons. J. Geophys. Res. 95, 21503–21521.
Eggins, J., Hensen, B.J., 1987. Evolution of mantle-derived, augite–hypersthene granodiorites by crystal–liquid fractionation: Barrington Tops batholith, eastern Australia. Lithos 20, 295–310.
Fan, W.M., Wang, Y.J., Zhang, A.M., Zhang, F.F., Zhang, Y.Z., 2010. Permian arc–back-arc basin development along the Ailaoshan tectonic zone: geochemical, isotopic and geochronological evidence from the Mojiang volcanic rocks, southwest China. Lithos 119, 553–568.
Friedman, I., O'Neil, J.R., 1977. Compilation of Stable Isotope Fractionation Factors of Geochemical Interest. Data of Geochemistry. U.S. Geological Survey Professional Paper, 440-KK, pp. 1–12.
Grove, T.L., Donnelly-Nolan, J.M., 1986. The evolution of young silicic lavas at Medicine Lake Volcano, California: implications for the origin of compositional gaps in calc-alkaline series lavas. Contrib. Mineral. Petrol. 92, 281–302.
Guffanti, M., Clynne, M.A., Muffler, L.J.P., 1996. Thermal and mass implications of magmatic evolution in the Lassen volcanic region, California, and constraints on basalt influx to the lower crust. J. Geophys. Res. 101, 3001–3013.
Han, B.F., Wang, S.G., Jahn, B.M., Hong, D.W., Kagami, H., Sun, Y.L., 1997. Depleted-mantle source for the Ulungur River A-type granites from North Xinjiang, China: geochemistry and Nd–Sr isotopic evidence, and implications for Phanerozoic crustal growth. Chem. Geol. 138, 135–159.
Hart, T.R., Gibson, H.L., Lesher, C.M., 2004. Trace element geochemistry and petrogenesis of felsic volcanic rocks associated with volcanogenic massive Cu–Zn–Pb sulfide deposits. Econ. Geol. 99, 1003–1013.
Hennig, D., Lehmann, B., Frei, D., Belyatsky, B., Zhao, X.F., Cabral, A.R., Zeng, P.S., Zhou, M.F., Schmidt, K., 2009. Early Permian seafloor to continental arc magmatism in the eastern Paleo-Tethys: U–Pb age and Nd–Sr isotope data from the southern Lancangjiang zone, Yunnan, China. Lithos 113, 408–422.
Heppe, K., 2004. Plate Tectonic Evolution and Mineral Resource Potential of the Lancang River Zone, Southwestern Yunnan, People's Republic of China (Thesis) University of Göttingen, Göttingen, Germany, pp. 1–147.
Huang, X.W., Zhao, X.F., Qi, L., Zhou, M.F., 2013. Re–Os and S isotopic constraints on the origins of two mineralization events at the Tangdan sedimentary rock-hosted stratiform Cu deposit, SW China. Chem. Geol. 347, 9–19.
Irvine, T.N., Baragar, W.R.A., 1971. A guide to the chemical classification of the common volcanic rocks. Can. J. Earth Sci. 8, 523–548.
Jian, P., Liu, D.Y., Kröner, A., Zhang, Q., Wang, Y.Z., Sun, X.M., Zhang, W., 2009a. Devonian to Permian plate tectonic cycle of the Paleo-Tethys orogen in southwest China (I): geochemistry of ophiolites, arc/back-arc assemblages and within-plate igneous rocks. Lithos 113, 748–766.
Jian, P., Liu, D.Y., Kröner, A., Zhang, Q., Wang, Y.Z., Sun, X.M., Zhang, W., 2009b. Devonian to Permian plate tectonic cycle of the Paleo-Tethys orogen in southwest China (II): insights from zircon ages of ophiolites, arc/back-arc assemblages and within-plate igneous rocks and generation of the Emeishan CFB province. Lithos 113, 767–784.
Jian, P., Liu, D.Y., Sun, X.M., 2003. SHRIMP dating of Baimaxueshan and Ludian granitoid batholiths northwestern Yunnan province, and its geological implications. Acta Geosci. Sin. 24 (4), 338–342 (in Chinese with English abstract).
Jian, P., Liu, D.Y., Sun, X.M., 2004. SHRIMP dating of Jicha Alaskan-type gabbro in western Yunnan province: evidence for the early Permian subduction. Acta Geol. Sin. 78, 165–170.
Jian, P., Liu, D.Y., Sun, X.M., 2008. SHRIMP dating of the Permo-Carboniferous Jinshajiang ophiolite, southwestern China: geochronological constraints for the evolution of Paleo-Tethys. J. Asian Earth Sci. 32, 371–384.
Kelly, W.C., Rye, R.O., 1979. Geologic, fluid inclusion, and stable isotope studies of the tin-tungsten deposits of Panasqueira, Portugal. Econ. Geol. 74, 1721–1822.
Le Bas, M.J., Streckeisen, A.L., 1991. The IUGS systematics of igneous rocks. J. Geol. Soc. Lond. 148, 825–833.
Lehmann, B., Zhao, X.F., Zhou, M.F., Du, A.D., Mao, J.W., Zeng, P.S., Henjes-Kunst, F., Heppe, K., 2013. Mid-Silurian back-arc spreading at the northeastern margin of gondwana: the Dapingzhang dacite-hosted massive sulfide deposit, Lancangjiang zone, southwestern Yunnan, China. Gondwana Res. 24, 648–663.
Li, C., Dong, Y.S., Zhai, Q.G., Wang, L.Q., Yan, Q.R., Wu, Y.W., He, T.T., 2008. Discovery of Eopaleozoic ophiolite in the Qiangtang of Tibet Plateau: evidence from SHRIMP U–Pb dating and its tectonic implications. Acta Pet. Sin. 24, 31–36 (in Chinese with English abstract).
Li, F., Zhuang, F.L., 2000. Geological characteristics and its genesis of Dapingzhang Cu-polymetal deposit in western Yunnan. J. Kunming Univ. Sci. Technol. (Nat. Sci.) 25, 32–36 (in Chinese with English abstract).
Li, F., Zhuang, F.L., 2001. Volcanic–echalative–sedimentary genesis of Fapingzhang Cu-polymetal deposit in western Yunnan. Geophys. Prospect. 37, 5–8 (in Chinese with English abstract).
Li, F., Zhuang, F.L., Yang, H.L., 2000. Fluid inclusion characteristics of Dapingzhang Cu-polymetal deposit in western Yunnan. Acta Pet. Sin. 16, 581–586 (in Chinese with English abstract).
Li, G.Z., Li, C.S., Ripley, E.M., Kamo, S., Su, S.G., 2012. Geochronology, petrology and geochemistry of the Nanlinshan and Banpo mafic–ultramafic intrusions: implications for subduction initiation in the eastern Paleo-Tethys. Contrib. Mineral. Petrol. 164, 773–788.
Li, X.H., Li, W.X., Li, Z.X., Lo, C.H., Wang, J., Ye, M.F., Yang, Y.H., 2009. Amalgamation between the Yangtze and Cathaysia Blocks in South China: constraints from SHRIMP U–Pb zircon ages, geochemistry and Nd–Hf isotopes of the Shuangxiwu volcanic rocks. Precambrian Res. 174, 117–128.
Liu, C.S., Zhu, J.C., 1989. Quantitative modeling source rocks of Lincang granite batholith, west Yunnan. Acta Petrol. Mineral. 8, 1–12 (in Chinese with English abstract).
Ludwig, K.R., 2003. Isoplot/Ex Version 3.23. A Geochronological Toolkit for Microsoft Excel. Berkeley Geochronology Center (Special Publication).
Lugmair, G.W., Harti, K., 1978. Lunar initial $^{143}Nd/^{144}Nd$: differential evolution of the lunar crust and mantle. Earth Planet. Sci. Lett. 39, 349–357.
Mao, X.C., Wang, L.Q., Li, B., Wang, B.D., Wang, D.B., Yin, F.G., Sun, Z.M., 2012. Discovery of the late Silurian volcanic rocks in the Dazhonghe area, Yunxian–Jinggu volcanic arc

belt, western Yunnan, China and its geological significance. Acta Pet. Sin. 28, 1517–1528 (in Chinese with English abstract).
Martin, H., Bonin, B., Capdevila, R., Jahn, B.M., Lameyre, J., Wang, Y., 1994. The Kuiqi peralkaline granitic complex (SE China): petrology and geochemistry. J. Petrol. 35, 983–1015.
Matsuhisa, Y., Goldsmit, J.R., Clyton, R.N., 1979. Oxygen isotopic fractionation in the system quartz–albite–anorthite–water. Geochim. Cosmochim. Acta 43, 1131–1140.
Metcalfe, I., 2002. Permian tectonic framework and palaeogeography of SE Asia. J. Asian Earth Sci. 20, 551–566.
Metcalfe, I., 2011. Palaeozoic–Mesozoic history of SE Asia. Geol. Soc. Lond. Spec. Publ. 355, 7–35.
Mo, X.X., Pan, G.T., 2006. From the Tethys to the formation of the Qinghai–Tibet plateau: constrained by tectono-magmatic events. Earth Sci. Front. 13, 43–51 (in Chinese with English abstract).
Mo, X.X., Lu, F.X., Shen, S.Y., Zhu, Q.W., Hou, Z.Q., Yang, K.H., Deng, J.F., Liu, X.P., He, C.X., Lin, P.Y., Zhang, B.M., Tai, D.Q., Chen, M.H., Hu, X.S., Ye, S., Xue, Y.X., Tan, J., Wei, Q.R., Fan, L., 1993. Sanjiang Tethyan Volcanism and Related Mineralization. Geological Publishing House, Beijing, p. 276 (in Chinese).
Mo, X.X., Shen, S.Y., Zhu, Q.W., 1998. Volcanics-ophiolite and Mineralization of Middle and Southern Part in Sanjiang, Southern China. Geological Publishing House, Beijing, pp. 1–128 (in Chinese).
Ohmoto, H., 1972. Systematics of sulfur and carbon isotopes in hydrothermal ore deposits. Econ. Geol. 67, 551–579.
Ohmoto, H., 1986. Stable isotope geochemistry of ore deposits. Rev. Mineral. 16, 491–560.
Pan, G.T., Li, X.Z., Wang, L.Q., Ding, J., Chen, Z.L., 2002. Preliminary division of tectonic units of Qinghai–Tiber plateau and its adjacent regions. Geol. Bull. China 21, 701–707 (in Chinese with English abstract).
Pan, G.T., Xu, Q., Hou, Z.Q., Wang, L.Q., Du, D.X., Mo, X.X., Li, D.M., Wang, M.J., Li, X.Z., Jiang, X.S., 2003. Archipelagic Orogenesis, Metallogenic Systems and Assessment of the Mineral Resources Along the Nujing–Langcangjiang–Jinshajiang Area in Southwestern China. Geological Publishing House, Beijing, pp. 1–420 (in Chinese).
Pearce, J.A., Harris, N.B.W., Tindle, A.G., 1984. Trace element discrimination diagrams for the tectonic interpretation of granitic rocks. J. Petrol. 25, 956–983.
Peng, T.P., Wang, Y.J., Fan, W.M., Liu, D.Y., Shi, Y.R., Miao, L.C., 2006. SHRIMP zircon U–Pb geochronology of early Mesozoic felsic igneous rocks from the southern Lancangjiang and its tectonic implications. Sci. China Ser. D Earth Sci. 49, 1032–1042.
Peng, T.P., Wang, Y.J., Zhao, G.C., Fan, W.M., Peng, B.X., 2008. Arc-like volcanic rocks from the southern Lancangjiang zone, SW China: geochronological and geochemical constraints on their petrogenesis and tectonic implications. Lithos 102, 358–373.
Peng, T.P., Wilde, S.A., Wang, Y.J., Fan, W.M., Peng, B.X., 2013. Mid-Triassic felsic igneous rocks from the southern Lancangjiang zone, SW China: petrogenesis and implications for the evolution of Paleo-Tethys. Lithos 168–169, 15–32.
Qi, L., Hu, J., Grégoire, D.C., 2000. Determination of trace elements in granites by inductively coupled plasma mass spectrometry. Talanta 51, 507–513.
Qi, L., Zhou, M.F., Gao, J., Zhao, Z., 2010. An improved Carius tube technique for determination of low concentrations of Re and Os in pyrites. J. Anal. At. Spectrom. 25, 585–589.
Rapp, R.P., Watson, E.B., 1995. Dehydration melting of metabasalt at 8–32 kbar: implications for continental growth and crust–mantle recycling. J. Petrol. 36, 891–931.
Rickwood, P.C., 1989. Boundary lines within petrologic diagrams which use oxides of major and minor elements. Lithos 22, 247–263.
Ru, S.S., Li, F., Wu, J., Li, J.B., Wang, D.W., Huang, Y.C., 2012. Geochemistry and chronology of granodiorite porphyry in the Dapingzhang Cu polymetallic deposit. Acta Petrol. Mineral. 31, 531–540 (in Chinese with English abstract).
Rushmer, T., 1991. Partial melting of two amphibolites: contrasting experimental results under fluid absent conditions. Contrib. Mineral. Petrol. 107, 41–59.
Shen, S.Y., Feng, Q.L., Liu, B.P., Mo, X.X., 2002. Study on ocean ridge, ocean island volcanic rocks of Changning–Menglian belt. Geol. Sci. Technol. Inform. 21, 13–17 (in Chinese with English abstract).
Smoliar, M.I., Walker, R.J., Morgan, J.W., 1996. Re–Os ages of group IIA, IIIA, IVA, and IVB iron meteorites. Science 271, 1099–1102.
Steiger, R.H., Jäger, E., 1977. Subcommission on geochronology: convention on the use of decay constants in geo- and cosmochronology. Earth Planet. Sci. Lett. 36, 359–362.
Stein, H.J., Morgan, J.W., Schersten, A., 2000. Re–Os dating of low-level highly radiogenic (LLHR) sulfides: the Harnäs gold deposit, southwest Sweden, records continental-scale tectonic events. Econ. Geol. 95, 1657–1671.
Sun, S.-S., McDonough, W.F., 1989. Chemical and Isotopic Systematics of Oceanic Basalts: Implications for Mantle Composition and Processes. In: Saunders, A.D., Norry, M.J. (Eds.), Magmatism in the Ocean Basins. Geol. Soc. London, Special Publications no. 42, pp. 313–345.
Taylor, H.P., 1979. Oxygen and Hydrogen Isotope Relations in Hydrothermal Ore Deposits. In: Barnes (Ed.), Geochemistry of Hydrothermal Ore Deposits. Wiley, New York, pp. 236–277.
Tepper, J.H., Nelson, B.K., Bergantz, G.W., Irving, A.J., 1993. Petrology of the Chilliwack Batholith, North Cascades, Washington; generation of calc-alkaline granitoids by melting of mafic lower crust with variable water fugacity. Contrib. Mineral. Petrol. 113, 333–351.
Vezier, J., Hoefs, J., 1976. The nature of O^{18}/O^{16} and C^{13}/C^{12} secular trends in sedimentary carbonate rocks. Geochim. Cosmochim. Acta 40, 1387–1395.
Wan, D.F., Fan, T.Y., Tian, S.H., 2005. The chromiuman analytical technique for hydrogen isotopes. Acta Geosci. Sin. 26, 35–38 (Sup., in Chinese with English abstract).
Wang, B.D., Wang, L.Q., Chen, J.L., Yin, F.G., Wang, B.D., Zhang, W.P., Chen, L.K., Liu, H., 2014. Triassic three-stage collision in the Paleo-Tethys: constraints from magmatism in the Jiangda–Deqen–Weixi continental margin arc, SW China. Gondwana Res. 26, 475–491.
Wang, B.D., Wang, L.Q., Pan, G.T., Yin, F.G., Wang, D.B., Yuan, T., 2013. U–Pb zircon dating of Early Paleozoic gabbro from the Nantinghe ophiolite in the Changning–Menglian suture zone and its geological implication. Chin. Sci. Bull. 58, 920–930.
Wang, J.B., 2004. Analysis and prospect of the copper resources in China. Chin. Bull. Metal. 47, 1–5.
Wang, L.Q., Pan, G.T., Li, C., Dong, Y.S., Zhu, D.C., Yuan, S.H., Zhu, T.X., 2008. SHRIMP U–Pb zircon dating of Eopaleozoic cumulative in Guoganjianian Mt. from central Qiangtang area of northern Tibet—considering the evolvement of Proto- and Paleo-Tethys. Geol. Bull. China 27, 2045–2056 (in Chinese with English abstract).
Wang, Y.J., Zhang, A.M., Fan, W.M., Peng, T.P., Zhang, F.F., Zhang, Y.H., Bi, X.W., 2010. Petrogenesis of late Triassic post-collisional basaltic rocks of the Lancangjiang tectonic zone, southwest China, and tectonic implications for the evolution of the eastern Paleotethys: geochronological and geochemical constraints. Lithos 120, 529–546.
Watson, E.B., Capobianco, C.J., 1981. Phosphorus and the rare earth elements in felsic magmas an assessment of the role of apatite. Geochim. Cosmochim. Acta 45, 2349–2358.
Wu, F.Y., Sun, D.Y., Li, H.M., Jahn, B.M., Wilde, S.A., 2002. A-type granites in northeastern China: age and geochemical constraints on their petrogenesis. Chem. Geol. 187, 143–173.
Xu, J.F., Castillo, P.R., 2004. Geochemical and Nd–Pb isotopic characteristics of the Tethyan asthenosphere: implications for the origin of the Indian Ocean mantle domain. Tectonophysics 393, 9–27.
Yang, G.L., 2003. Geology and genesis of Minle ash flow copper deposit. Yunnan Geol. 22, 80–88 (in Chinese with English abstract).
Yang, G.L., Hu, G.D., 2001. The geological characteristics and metallogenetic mechanism of Dapingzhang multimetallic Cu deposit, Simao. Yunnan Geol. 20, 347–360 (in Chinese with English abstract).
Yang, Y.Q., et al., 2000. Geological setting, metallogenic conditions and prediction of massive sulfide copper deposits in the volcanic belt of the southern Lancangjiang region, Yunnan province. Unpublished report, Institute of Mineral Deposits, Chinese Academy of Geological Sciences, and Number 5 Geological Brigade, Yunnan Bureau of Geology and Mineral Resources, Beijing and Kunming, 1–178 (in Chinese).
Yang, Z.L., 2004. Minle volcanic–subvolcanic copper deposit. Yunnan Geol. 23, 343–350 (in Chinese with English abstract).
Yang, W.Q., Feng, Q.L., Duan, X.D., 2007. Late Devonian pillow basalt and bedded chert in Chmagning–Mengnma tectonic belt of southwestern Yunnan, China. Geol. Bull. China 26, 739–747 (in Chinese with English abstract).
YBGMR (Yunnan Bureau of Geology and Mineral Resources), 1990. Regional Geology of Yunnan Province. Geological Publishing House, Beijing, pp. 1–728 (in Chinese).
YBGMR (Yunnan Bureau of Geology and Mineral Resources), 2001. Geological map 1: 200,000 of Dapingzhang-Jako area. No. 5 Geological Brigade, Simao/Kunming.
Zartman, R.E., Doe, B.R., 1981. Plumbotectonics—the model. Tectonophysics 75, 135–162.
Zhai, Q.G., Wang, J., Li, C., Su, L., 2010. SHRIMP U–Pb dating and Hf isotopic analyses of Middle Ordovician meta-cumulative gabbro in central Qiangtang, northern Tibetan Plateau. Sci. China Ser. D Earth Sci. 53, 657–664.
Zhang, Q., Li, D.Z., Zhang, K.W., 1985. Preliminary study on Tongchangjie ophiolite mélange from Yunnan Province. Acta Pet. Sin. 1, 1–14 (in Chinese with English abstract).
Zhang, Q., Zhang, K.W., Li, D.Z., Wu, H.W., 1988. A preliminary study of shuanggou ophiolite in Xinping county, Yunnan province. Acta Pet. Sin. 3, 37–48 (in Chinese with English abstract).
Zhao, D.X., 1990. Age and formational environment of metamorphosed volcano-sedimentary rocks of Damenglong Group, SW Yunnan. Yunnan Geol. 9, 107–116 (in Chinese with English abstract).
Zhong, D.L., 1998. The Paleotethys Orogenic Belt in West of Sichuan and Yunnan. Science Publishing House, Beijing, pp. 1–230 (in Chinese).
Zhong, D.L., Wu, G.Y., Ji, J.Q., Zhang, Q., Ding, L., 1998. The discovery of ophiolite in southeastern Yunnan (in Chinese). Chin. Sci. Bull. 43, 1365–1370 (Chinese Version, in Chinese).
Zhong, H., Hu, R.Z., Ye, Z.J., 2000. Sulfur, lead, hydrogen and oxygen isotopic geochemistry of the Dapingzhang copper-polymetallic deposit, Yunnan Province. Geochimica 29, 136–142 (in Chinese with English abstract).
Zhong, H., Hu, R.Z., Ye, Z.J., 2001. Preliminary study on origin of ore-forming materials in Dapingzhang copper-metallic deposit, Yunnan province. Chin. J. Geol. 36, 72–82 (in Chinese with English abstract).
Zhu, W.G., Zhong, H., Wang, L.Q., He, D.F., Ren, T., Fan, H.P., Bai, Z.J., 2011. Petrogenesis of the basaltic rocks and rhyolite porphyries of the Minle copper deposit, Yunnan: geochronological and geochemical constraints. Acta Pet. Sin. 27, 2694–2708 (in Chinese with English abstract).